Hindawi
Advances in Materials Science and Engineering
Volume 2019, Article ID 4251953, 21 pages
https://doi.org/10.1155/2019/4251953

Review Article

Solid-State Processing Route, Mechanical Behaviour, and Oxidation Resistance of TiAl Alloys

Prince V. Cobbinah and Wallace R. Matizamhuka

Department of Metallurgical Engineering, Vaal University of Technology, Andries Potgieter Blvd, Vanderbijlpark, Gauteng 1911, South Africa

Correspondence should be addressed to Prince V. Cobbinah; prinzcobbs@gmail.com

Received 29 May 2019; Revised 6 September 2019; Accepted 25 September 2019; Published 20 October 2019

Academic Editor: Michael Aizenshtein

A primary challenge associated with TiAl alloys is their low ductility at room temperature. One approach to overcome this flaw is attaining ultrafine grains in the alloy's final microstructure. The powder metallurgy (PM) processing route favours the synthesising of ultrafine grains in TiAl alloys. This paper features the mechanical alloying (MA) process and rapid consolidation through the spark plasma sintering (SPS) technique, which comprises the PM process. Furthermore, a second approach discussed covers microalloying TiAl alloys. An evaluation of the influence of high oxygen content is also presented, including the formation of α-Al_2O_3. A section of the review delves into the dynamic recrystallisation mechanisms involved in elevated temperature deformation of TiAl alloys. The final section highlights the efficacy of ternary element additions to TiAl alloys against oxidation.

1. Introduction

Intermetallics are described as an ordered alloy phase formed between two metallic elements. An alloy is said to be ordered provided two or more sublattices are needed to describe its atomic structure [1]. Titanium aluminides (TiAl), over the years, have been some of the most interesting and highly researched lightweight structural materials. They have been envisaged in replacing nickel-based superalloys (NBSAs) for certain stress and temperature application ranges. The alloy design concept is quite similar to that of NBSAs. Titanium aluminides exhibit an ordered α_2(Ti_3Al) and γ(TiAl) phases, analogous to that of NBSA's $L1_2$ ordered phase. Additionally, TiAl alloys exhibit a combination of enviable properties such as low density (~3.9–4.2 $g{\cdot}cm^{-3}$), high melting point of 1733 K, high strength to weight ratio (up to 1000 MPa) that can be retained at temperatures up to 973 K, high elastic moduli, low diffusion coefficient, good creep properties up to 1173 K, and substantial resistance to corrosion and oxidation. Additionally, compared to ceramics, they exhibit good thermal conductivities and are ductile at their service temperatures while also maintaining good structural stability [2, 3].

2. Applications

Owing to the weight-saving property, *inter alia* other properties of titanium aluminides, it has found significant use primarily in the aerospace sector [4, 5]. So far, it has successfully been used for components in gas turbine engines where it is predicted to save weight to about 20% when used for small parts (blades, vanes, and shrouds) and about 49% when used in casings. Major turbine engine manufacturers in the industry have recognised the potential of TiAl alloys. General Electric (GE) currently uses TiAl alloys, specifically the second-generation Ti-48Al-2Cr-2Nb (at.%), for low-pressure turbine (LPT) blades in the GEnx™ used by Boeing's 787s and 747-8s aeroplanes as shown in Figure 1. Also, SNECMA uses the same second-generation alloy for their LEAP™ engine LPT blades [6]. Pratt and Whitney and Volvo have subjected TiAl-based alloys to several rigorous tests and through their demonstrations have shown their capabilities to be used for shrouds, blade retainers, and turbine dampers [6]. The automotive industry is another sector where TiAl alloys have received increasing attention. It is used for turbine wheels of turbochargers for diesel or gasoline engines in sports cars and passenger vehicles as

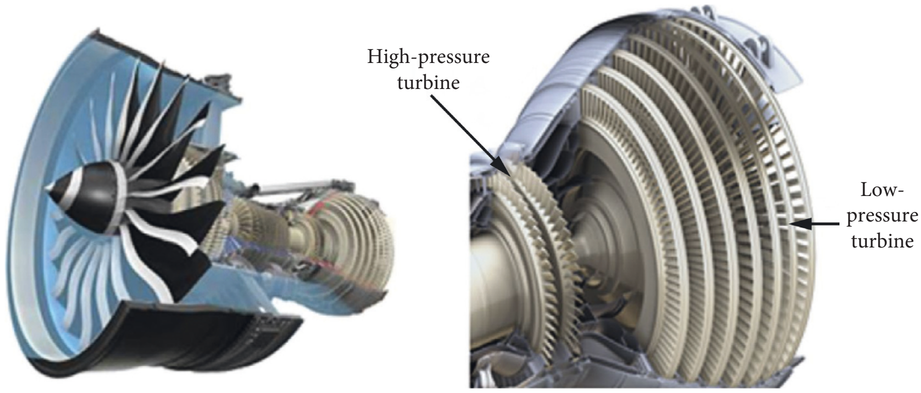

(a)

(b)

FIGURE 1: (a) Diagrams showing the complete engine and the turbine section of the GEnx-1B aircraft engine as used on the Boeing 787. (b) Photograph of TiAl LPT blade as used in the last stage of GEnx engine and an assembly of TiAl LPT blades after an engine test as used in the GE CF6 test engine [6].

depicted in Figure 2 (such as Mitsubishi motors Lancer 6 model) [7]. Also, it is used for exhaust valves for high-performance racing cars [8].

3. Phases and Microstructure Evolutions

According to the phase diagram (Figure 3), TiAl alloys on solidifying goes through the single-phase region of the α solid solution and, on further cooling, decomposes according to the reactions, $\alpha \longrightarrow \alpha + \gamma \longrightarrow \alpha_2 + \gamma$ or $\alpha \longrightarrow \alpha_2 \longrightarrow \alpha_2 + \gamma$. Depending on the cooling rate, different phase transformations can occur, and a variety of microstructures can be attained. This gives the opportunity of controlling the microstructures to gain specific properties for peculiar applications.

The α_2-Ti_3Al phase transforms from a disordered to an ordered phase in the range of 22 to 39 at.% Al at around 1453 K. The α_2 ordered phase has a hexagonal crystal structure (DO_{19}) with lattice parameters, $a = 0.5782$ nm and $c = 0.4629$ nm, as shown in Figure 4(a). It is known to exhibit a good high-temperature strength but with very low ductility. Additionally, it has a high rate of oxygen and hydrogen absorption, which at high temperature results in embrittlement of the alloy [9].

From 49 to 66 at.% Al, the γ-TiAl phase is stable and evaluated as ordered up to its melting temperature [3]. The phase has an ordered face-centred tetragonal structure ($L1_0$) with lattice $a = 0.4005$ nm and $c = 0.4070$ nm. It exhibits a tetragonality (c/a) of 1.02 (Figure 4(b)) at the equiatomic position, and this appreciates to 1.03 at increasing Al proportions [1]. It has an extremely low ductility at room temperature owing to the limited number of slip systems [10].

On the other hand, it exhibits excellent resistance to oxidation. Furthermore, the covalent bonds of atoms in the γ-TiAl phase translate to high specific strength and modulus associated with the phase [12]. Compared to the α_2-Ti_3Al phase, the γ-TiAl phase is lighter and can be used at higher temperatures.

Alloys with duplex phases, more specifically $\alpha_2 + \gamma$, are preferred for structural engineering applications. This is due to the flexibility in controlling the proportions of formed α_2 and γ phases, together with their distribution [13]. Grain morphology greatly varies depending on composition, temperature and time, cooling rate, and stabilisation temperature and time [13].

As shown in Figure 5, there are four different classifications of microstructures associated with the dual-phase TiAl alloys. They are near gamma (NG), near lamellar (NL), fully lamellar (FL), and the duplex microstructures (DM) [14].

The fully lamellar (FL) microstructure forms when fabrication temperature or heat treatment is carried out at a temperature within the pure α-phase field and cooled to room temperature. During cooling, formed α-Ti precipitates into alternating layers of α (orders to α_2) and γ with a lamellar morphology. The grains of the microstructure are coarse and range from 200 to 1000 μm [15].

The duplex microstructure (DM) occurs when fabrication temperature or heat treatment is carried out at a

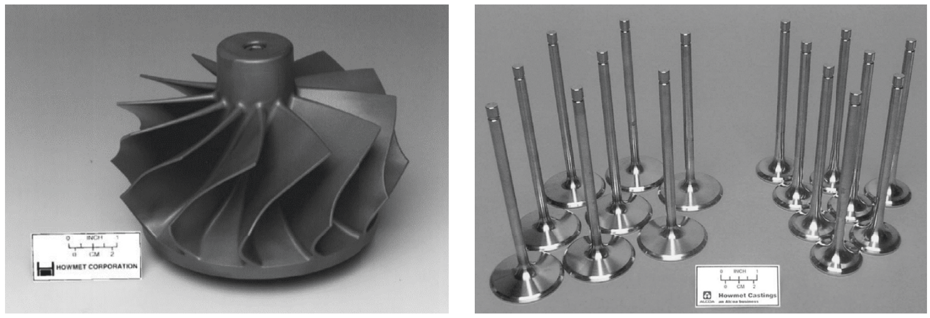

(a) (b)

Figure 2: (a) Turbine wheel casting of γ-TiAl for automotive turbochargers by Howmet Corporation. (b) Cast γ-TiAl exhaust valves in testing for high-performance cars [8].

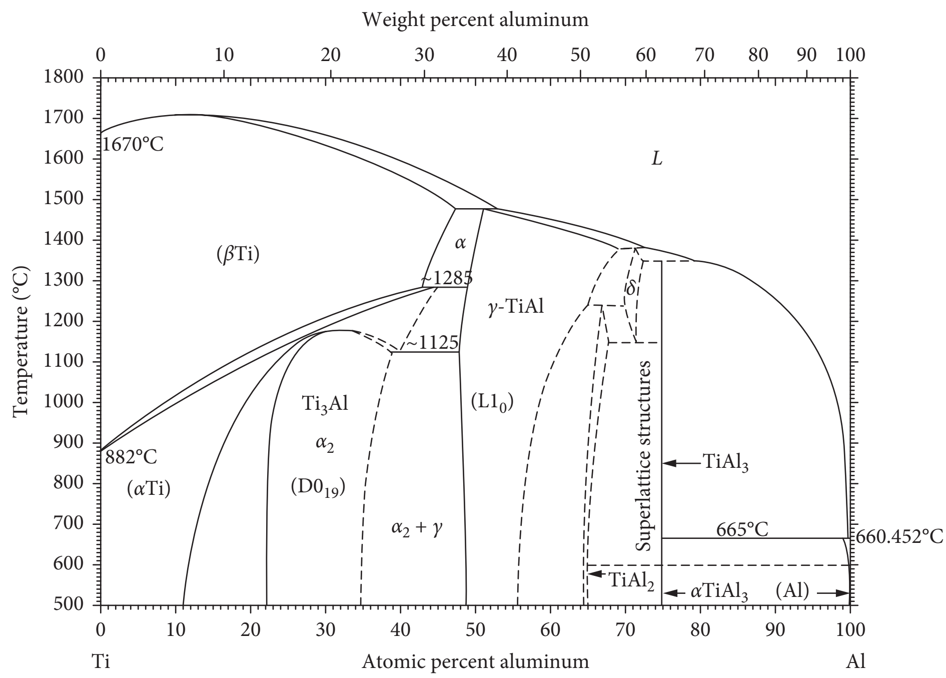

Figure 3: Binary phase diagram of TiAl alloy [3].

temperature within the $\alpha + \gamma$-phase field. Equiaxed γ grains and fine lamellar colonies of alternating plates of α_2- and γ-phase characterise the duplex microstructure [17].

The near lamellar (NL) microstructure forms within the $\alpha + \gamma$-phase field close to the α-transus at temperatures between the duplex and fully lamellar. It consists of some equiaxed γ grains and mainly $\alpha_2 + \gamma$ lamellar grains [11].

The near gamma (NG) microstructure is obtained in the $\alpha_2 + \gamma$-phase region below the eutectoid temperature. The microstructure is made up of equiaxed γ grains with α_2 precipitates at the grain boundaries and triple points. The microstructure is characterised by mean grain size, usually between 30 μm and 50 μm [15, 18].

4. Alloy Development

The major challenge associated with TiAl alloys is its low ductility at ambient temperatures. Over the years to date, a lot of efforts have and are channelled in improving this mechanical property. Some include (i) microalloying to form ternary or quaternary alloys (Section 4); (ii) grain refinement through the powder metallurgy processing route or by rapid solidification (Sections 5 and 6) [19–21]; (iii) alteration of the morphology, volume fraction, and distribution of constituent phases by heat treatment [19, 22, 23].

4.1. Microalloying of TiAl Alloys. There have been several composition ranges studied in an attempt to improve ductility and/or a combination of other properties in TiAl alloys. The second-generation compositions of TiAl alloys in at.% are represented as follows:

(i) (45–52)Ti-(45–48)Al-(1–3)X-(2–5)Y-(<1)Z where X = (Cr, Mn, and V), Y = (Nb, Ta, W, and Mo), and Z = (B, C, and Y) [15, 24]

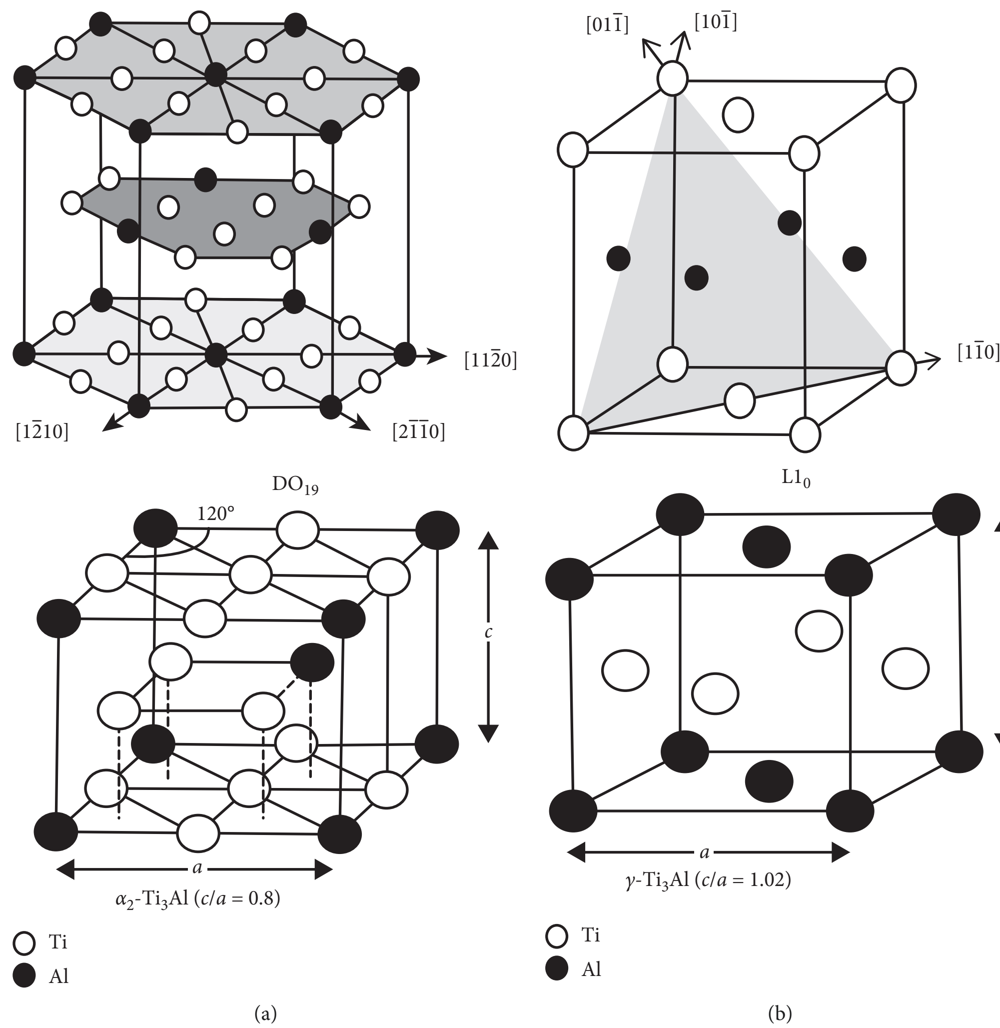

Figure 4: (a) Hexagonal crystal structure (DO_{19}) of α_2-Ti_3Al phase. (b) Face-centred tetragonal structure ($L1_0$) of γ-TiAl phase [11].

The third-generation composition includes the following:

(i) Ti-(42–48)Al-(0–10)X-(0–3)Y-(0–1)Z-(0–0.5RE), where X = (Cr, Mn, Nb, and Ta), Y = (Mo, W, Hf, and Zr); Z = (C, B, and Si). RE refers to rare earth elements [13, 16].

4.1.1. "X"-Elements Additions. The "X" elements are usually added to improve the mechanical properties of TiAl alloys through solid solution strengthening and/or precipitation hardening and also enhance ductility. Some include Nb, Cr, Mn, and V.

Nb is one element of interest present in all the compositions ranges. It has proven to enhance high-temperature strength and room temperature ductility [25, 26] but with decreased amounts of Al by shifting the α-phase boundary to the left [27]. As a β-stabilising element, Nb alters the β-phase region of the Ti-Al system and significantly increases the eutectoid temperature ($\alpha \longrightarrow \alpha_2 + \gamma$) [16]. These findings in recent years have significantly influenced academic dialogues on a new class of TiAl alloys termed "TNB" [3, 28–32] and "TNM" [23, 33–36] alloys. The concentration of Nb and/or Mo in these alloys is usually ≤ 10 at.% and includes small additions of B and C. In parallel, the addition of Nb and other BCC metals tends to modify the crystal structure of TiAl alloys to a more symmetric cubic lattice to attain the minimum number of slip systems required for plasticity, thus increasing ductility [37].

The addition of Cr and Mn has similar influence on TiAl alloys. Both elements lead to chemical strengthening (stacking fault interactions) owing to their preferential solubility in the HCP structure of TiAl alloys. As their concentration increases in TiAl alloys, they decrease the stacking fault energy and thereby further increase the separation of partial dislocations, resulting in improved ductility at elevated temperature [15, 38]. Additionally, Cr and Mn contents have been found to enhance room temperature ductility by altering the innate microstructure of TiAl-based alloys which are made apparent in decreasing the γ-TiAl phase tetragonality ratio (c/a) and unit-cell volume [39, 40], weakening the covalent directional Al_p–Ti_d bonds and reducing the volume fraction of the α_2-Ti_3Al phase [41].

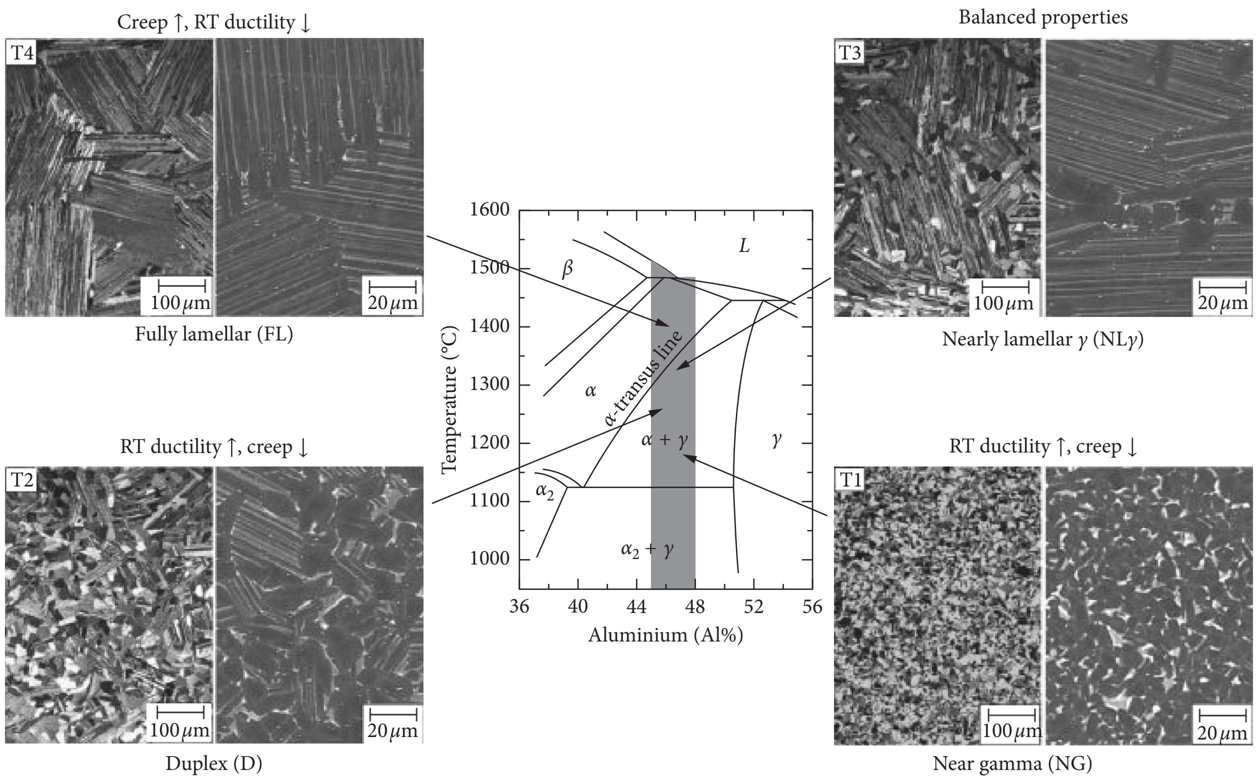

Figure 5: Midsection of the binary Ti-Al phase diagram and representative microstructures obtained through heat treatments within the α- and $(\alpha + \gamma)$-phase field. Note that the left half of the microstructural image represents a light-optical microscope (OM) image, whereas the right half is an SEM image taken in BSE mode, i.e., γ-TiAl appears dark, whereas α_2-Ti_3Al shows a light contrast. Heat treatments: little above the eutectoid temperature (T_{eu}) $\longrightarrow$ near gamma (NG) microstructure; between T_{eu} and α-transus temperature $T_\alpha \longrightarrow$ duplex (DM) microstructure. The volume fraction of lamellar grains depends on the heat treatment temperature relative to T_{eu} and T_α; just below $T_\alpha \longrightarrow$ nearly lamellar (NL) microstructure. The designation NL γ stands for a NL microstructure exhibiting a defined volume fraction of globular γ-grains, above $T_\alpha \longrightarrow$ FL microstructure (adopted from [16]).

4.1.2. "Y"-Elements Additions. Elements such as Zr, Mo, Ta, W, and Hf form the "Y" elements. These elements, because of their high-temperature refractory properties, hinder the diffusion processes in TiAl alloys by increasing the activation energy of diffusion and subsequently decreasing the dislocations climb rate. This enhances creep and thermal stability and promotes high-temperature performance [42]. Also, Hf and W improve the creep resistance of TiAl alloys with lamellar microstructures by segregating inside the α_2 lath close to the α_2/γ interface and hence stabilise the α_2/γ interface [43]. These elements are also known to stabilise the β-phase. The β-phase in TiAl alloys is regarded as a ductilising constituent. The β-phase has a BCC lattice which at elevated temperatures provides the adequate number of independent slip systems needed for ductility [44]. From weight and cost considerations, Ta, W, and Hf are less desired compared to Zr and Mo.

4.1.3. "Z"-Element Additions. The "Z" elements comprise low-density interstitial elements. They include C, B, Si, Y, and N. These elements form carbide, boride, silicide, and nitride precipitates. Carbon is a strong α-stabiliser and is known to lead to a change in phase evolution [45]. The addition of C improves the strengthening mechanisms of TiAl alloys. It has been shown to harden effectively both the α_2- and γ-phases leading to an increase in creep resistance and high-temperature strength [46]. Furthermore, C refines the lamellar microstructure of TiAl alloys by decreasing the lamellar spacing within the α_2/γ colonies formed upon cooling from the single α-phase region. The refinement of the lamellar microstructure is premised on the segregation of C atoms to initial α grain boundaries culminating in stacking fault energy reduction and therefore increases the frequency of fault formation [16]. Since the faults enhance the heterogeneous nucleation of γ-TiAl at grain boundaries, C effectively increases the nucleation rate of γ-TiAl, thus resulting in a fine lamellar structure [16]. The addition of B and Y to TiAl alloys serves as grain refining elements [24, 47, 48]. In good agreement with the Hall–Petch relationship, grain-refined microstructures enhance the mechanical properties of TiAl alloy [24]. Cheng et al. [49] asserted that increasing contents of interstitial B increases the strength of the duplex microstructure by impeding on dislocation through solute locking. The lamellar microstructure exhibits superior creep resistance because the aligned α-lamellae are strong barriers to dislocation mobility. Also, dislocation generated in the γ-phase accumulate at α_2/γ-interfaces [50]. In the case of Si, its influence on TiAl alloys has been contradicting. For example, Si form silicides

(ζ-Ti_5Si_3, $D8_8$ structure) either by the eutectic reaction of $L \longrightarrow \beta + \zeta$ (primary silicides) or by a eutectoid reaction of $\alpha_2 \longrightarrow \gamma + \zeta$ (secondary silicides) [23, 51]. These reactions depend on Si content and the alloy composition of the TiAl alloy in order to occur. These silicides enhance creep resistance by reducing dislocation mobility and also by stabilising the TiAl alloy microstructure against thermal degradation [52]. Conversely, alloying with Si has been suggested to produce extremely fine precipitates which act as weak barriers during creep. In conclusion, the presence of accumulated Si at the lamellar interfaces is argued to promote the introduction of vacancies and thus leads to destabilisation of the lamellar microstructure [53].

4.2. Presence of Oxygen. The microstructure of TiAl alloys is very sensitive to alloy compositions. The presence of interstitial elements, such as O, regarded as α-stabilising elements, are known to dissolve preferentially in the α-phase. Their increasing content tends to expand this phase field, raise the eutectoid temperature [54], and shift the peritectic reaction $L + \alpha \longrightarrow \gamma$ to higher Al content [55] as typified by the quasi-diagram in Figure 6.

During cooling, oxygen favours the chemical ordering of $\alpha \longrightarrow \alpha_2$ as a result of the significant difference in solubility of oxygen between the γ and α_2, with the equiaxed γ-phase unaltered [56]. This stems from the fact that interstitial elements, especially oxygen, search for convenient sites within the $L1_0$ structure of the γ-phase and the DO_{19} structure of the α_2-phase for optimum atomic neighbouring. Menand et al. [57] elaborated further that oxygen prefers the α_2-phase because of the octahedral sites of the DO_{19} structure. These octahedral sites are made up of two kinds of cavities; the Al_2Ti_4 type surrounded by two atoms of Al and four Ti atoms and the Ti_6 type with the cavities surrounded by six Ti atoms. The latter tend to be suitable for interstitial elements, in this case, for oxygen. Thus, the presence of high oxygen in the TiAl alloys influences diffusion, chemistry, and thermodynamic processes taking place in the alloy's microstructure formation. A higher oxygen content reduces ductility in TiAl alloys [50, 58]. However, the presence of the oxygen atoms tends to increasingly impede on the mobility of the ordinary dislocation resulting in strength improvement of TiAl alloys [50].

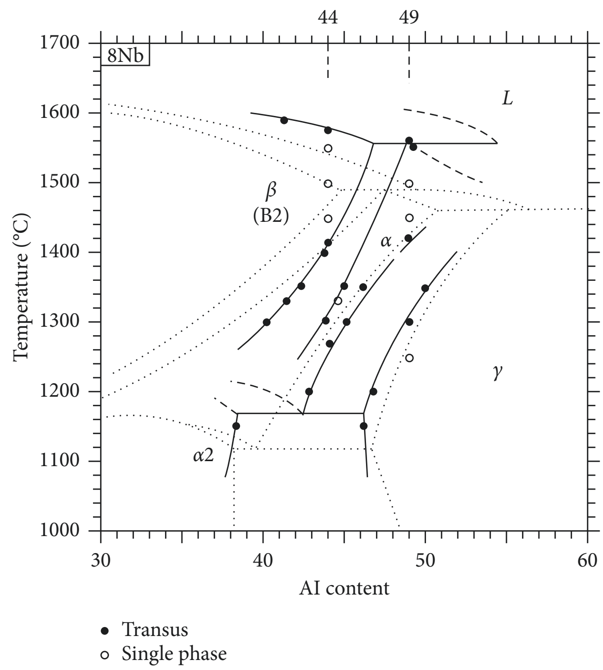

Figure 6: Quasi-phase diagram of TiAl-8Nb-xO [55].

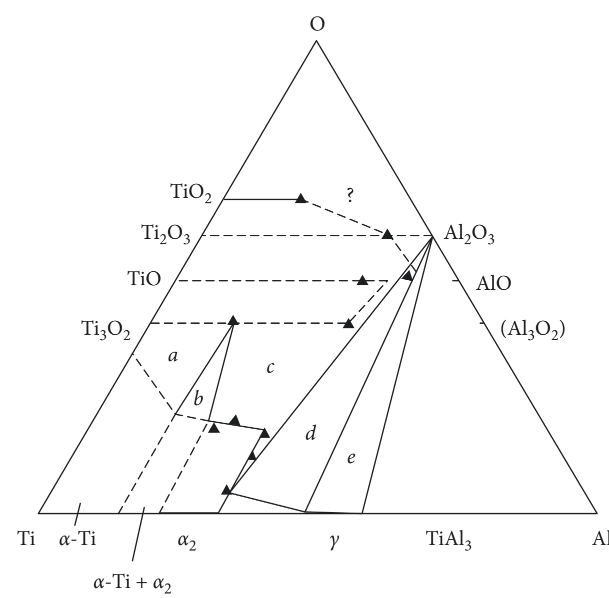

Figure 7: Incomplete phase diagram of Al-Ti-O based on experimental data. Coexisting phases in (a) α-(Ti, AI) + oxide; (b) α-(Ti, Al) + α_2-Ti_3Al + oxide; (c) α_2-Ti_3Al + oxide; (d) α_2-Ti_3Al + γ-TiAl + oxide; (e) γ-TiAl + oxide [(α-Ti,A1) = solid solution of Al in α-Ti] [62].

4.3. α-Al_2O_3 Formation. A likely source of oxygen addition in the processing of TiAl alloys is from their content in the starting Ti powder [59]. Additionally, the high-energy mechanical milling process, from other studies reported [60], leads to a significant increase in oxygen content which subsequently may result in an in situ reaction leading to the formation of α-Al_2O_3 particles [61]. In support, Rahmel et al. [62] reported that Al diffusion is faster than that of Ti in γ-TiAl alloys, since the ratio of diffusion coefficients D(Al)/D(Ti) = 2.7 [62]. Thus, the formed α-Al_2O_3 are promoted by high activities of Al and O in the TiAl alloy system. The formation of α-Al_2O_3 phase with the γ-TiAl and α_2-Ti_3Al phases is probable as reinforced by the phase diagram of Figure 7.

Along similar lines, the saturation of oxygen in the α-phase can result in the precipitation of α-Al_2O_3. Kawabata et al. [63] asserted that when the ratio of Ti/Al is <1 or Ti/Al ratio ≥ 1 with high oxygen content, the amount of oxygen present in the α-phase exceeds the solubility limit. After ordering to α_2, the oxygen content remains higher than the solubility limit. Thus, precipitation of α-Al_2O_3 occurs in the

α-phase, in α_2, and then in the γ-phase. Furthermore, in other instances where the ratio of Ti/Al >1 with medium oxygen content, oxygen atoms tend to form a solid solution in the α- and α_2-phases rather than precipitation. Solid solution of oxygen in the α-phase may stabilise the α-phase, which may suppress the $\alpha \longrightarrow \gamma$ transformation. Nevertheless, retardation of this transformation causes remaining α-phase to transform to α_2 by a short distance diffusion process [64].

The formation of α-Al_2O_3 during mechanical alloying has been reported to increase the efficiency of the process [65]. Also, the presence of α-Al_2O_3 in TiAl alloys, as suggested by Lapin et al. [50], contributes to the strengthening of the alloys.

5. Mechanical Alloying (MA)

The powder metallurgy (PM) processing route favours the synthesis of ultrafine, submicron, or nanograined microstructures and can be used in fabricating near-net-shape TiAl-based alloy products. The first stage of the PM process, wherein elemental metallic powders are blended or mixed, increases the tendency of attaining a homogeneous mixture before sintering. The process is achieved by mechanical means referred to as mechanical alloying (MA) or milling (MM). Mechanical alloying (MA) is defined as a solid-state powder processing technique involving essentially, repeated cold welding, fracturing, and rewelding of powders using high-energy ball mill equipment [66]. In the MA process, powders are plastically deformed under high-energy collision between balls and between balls and the wall of the container. As illustrated in Figure 8, the new surfaces formed during the collision promote cold welding of the powders, which are subsequently deformed plastically into a composite layered structure and eventually into new particles of different compositions. The laminate structure formation facilitates the dissolution of solute elements. According to Lü and Lai [10], the heat generated owing to the collision, lattice defects, and short diffusion distance promotes the dissolution of solute elements and formation of areas of solid solution throughout the powder matrix. Additionally, the deformation creates a high defect density, decreases the diffusion distance, and increases the powder temperature, which in the end enhances the diffusion rate. The powders undergo further fracturing and cold welding until very fine fully alloyed powders are attained with refined internal structures. For a successful MA, the right balance between the cold welding and fracturing processes is paramount [67].

The effect of mechanical milling and its process parameters in producing TiAl alloys have been studied [60, 68–72].

The state of the powders (milled or unmilled) prior to sintering affects the final microstructure of TiAl alloys [73, 74]. Mechanical milling increases the tendency of a homogeneous mixture of the α_2- and γ-phases owing to the high defect densities induced. These defect densities promote the nucleation of the α_2- and γ-phases. The milled powders produce ultrafine grains, and their densification takes place by grain boundary sliding aided by grain or surface boundaries diffusion. On the other hand, conventional plastic deformation by gliding and twinning is active for the coarse-grained unmilled powders [73]. The atmosphere under which mechanical alloying is carried out influences the production yield of TiAl powders. For instance, the introduction of nitrogen gas after milling in argon for a certain period, known as the nitrogen shock method, further assists the fracturing of the powders by forming brittle Al supersaturated α-phase solid-solution with nitrogen. The easy breakage of the formed brittle powders into fine particles results in an increase in the production yield [58, 75]. Furthermore, the tendency of attaining a homogeneous distribution of α_2 and γ grains in sintered TiAl-based alloys has also been shown to be favoured by an increase in rotation speed or milling time [74]. By increasing rotation speed or milling time, severe plastic deformation is likely to occur, leading to the buildup of large amounts of defect densities which favour phase transformation in the TiAl powder [74]. In addition, grinding ball sizes and the energy transferred by their impact affect solid-state reactions occurring during mechanical milling of TiAl-based alloys [76, 77]. The use of balls with different diameters in mechanical milling translates to high collision energy [10], which subsequently influences the structure of the MAed TiAl alloy. However, increasing the number of balls impacts negatively the performance of the milling process. Also, increasing the number of grinding balls raises the degree of filling of the mill causing low mobility in the balls and consequent reduction of kinetic energy transfer and milling efficiency [78]. An essential practical problem associated with the milling of TiAl alloys as well as other materials is the strong tendency of the powders sticking to the grinding media. Prolonged milling and high milling intensities presumably happen to increase the propensity of sticking due to the heating from impacts and friction, which makes the powder more ductile [60]. As a result, the severe sticking often culminates in poor microstructural homogeneity of the powders. Low milling intensity, however, slows the process of alloying [67, 77]. Process control agents (PCAs) are mostly added to help bring balance between fracture and cold welding of powders during milling, to suppress sticking. The introduction of PCAs or surfactants, which are mostly organic compounds, modifies the surfaces of deforming particles and minimises excessive cold welding. Depending on the type of PCA and milling conditions, a fraction of the PCA decomposes during milling and can contaminate the milled powders. Thus, low quantities are usually advised. Nonetheless, powder mixtures containing PCA can be pretreated by combustion synthesis (e.g., in a tube furnace) to extract the PCA before reaction occurs [79, 80]. The PCAs most commonly used in the milling of TiAl powders are benzene, stearic acid, and methanol [60, 80].

There are several studies on the constitution and structure of mechanically alloyed Ti-Al alloys. The formation of metastable FCC crystalline structures [10, 76, 81] and the formation of an amorphous phase [82–85] have all been reported.

6. Spark Plasma Sintering (SPS)

Spark plasma sintering (SPS) is a rapid densification technique wherein powders are consolidated through the

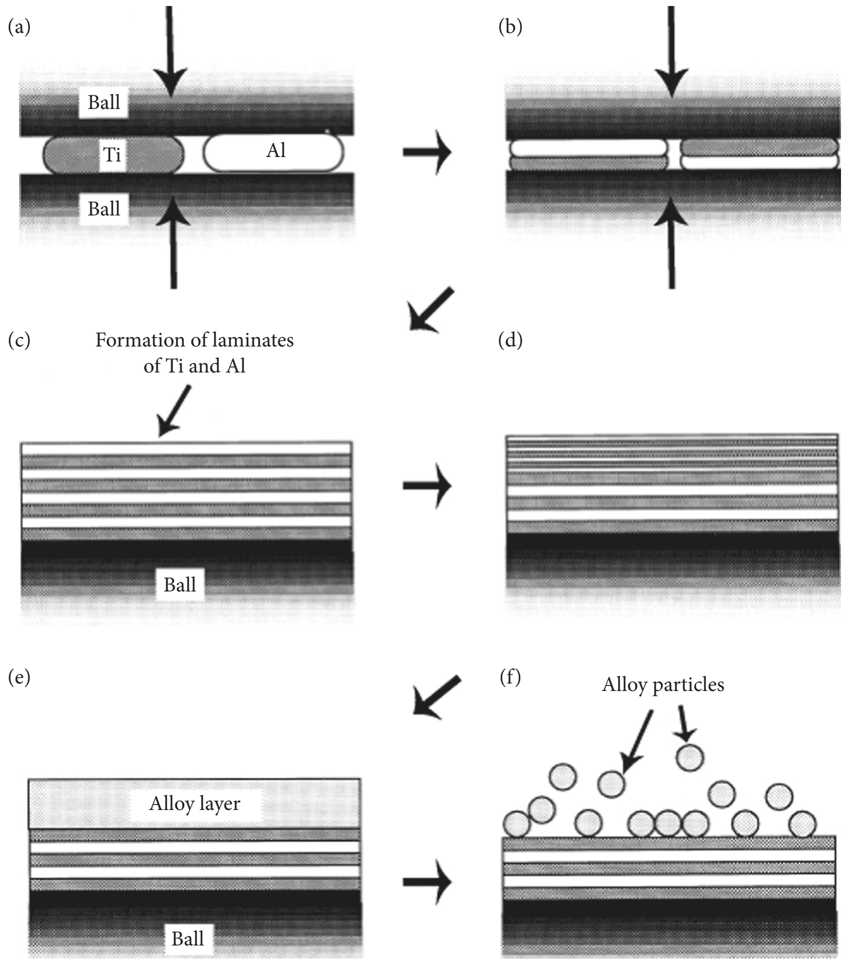

Figure 8: Schematic illustration showing the mechanical alloying process of Ti and Al: (a) formation of flaky Ti and Al particles by ball impact; (b) cold welding of flaky particles on ball surfaces and mill container wall; (c) formation of laminates of Ti and Al on milling balls and container wall; (d) refinement of layered structure of the laminates; (e) formation of alloy layer on the surface of laminates; (f) formation of alloy particles by breakage of the alloy layer, as adopted from [58].

simultaneous application of electric current or electric field and uniaxial pressure as depicted in Figure 9. Figure 9 outlines the principal components of a typical SPS system. It is made up of a uniaxial pressing device mainly the electrodes or punches, a water-cooled vacuum chamber and atmosphere controls, a water-cooled reaction chamber, a pulsed DC generator, and regulatory systems working together with appropriate software installed on a connected computer [86].

Foremost, in the early stages of sintering, the initial application of pressure leads to the compaction of the loose powders. This causes an increase in the contact area between powder particles and, consequently, strain hardening of the particles as the pressure further increases. Sintering mechanisms for metal powders are mainly diffusion processes at the surface, grain boundaries, and lattice paths [87]. However, at the surfaces of metallic powders, there exist microscopic or submicroscopic oxide films which tend to hinder the intercrystalline diffusion of the particles [88]. Hence, the heat needed for the fusion of the contacting surfaces is provided by the application of electric current, as shown in Figure 10. As the electric current is applied, it produces sparks owing to the accumulation of high temperature at the contacting areas [89]. The spark discharges tend to break down the resistance of the surface oxides on the powders. This phenomenon is termed Joule or resistive heating of the particles. Consequently, the occurrence of Joule heating at the contact areas of the particles leads to the exposure of a fresh metal surface of higher energy state relative to the internal energy of the particles [89]. There is a reduction in surface energy as the surface crystals of the contacting surfaces coalesce as in diffusion bonding and form conductive links. However, still in this plastically deformable state, the powder compacts take the shape of the mould while mechanical pressure is simultaneously applied [88].

To better comprehend the microstructure formations and associated properties of TiAl-based alloys, the densification mechanisms and kinetics involved in the SPS process have been studied at both macroscopic and microscopic levels. Of scrutiny in these studies has to do with one of the parameters essential to the SPS process. The next paragraph looks at some examples.

Lagos and Agote [90] studied the influence of different applied loads in the densification process of the 48-2-2 alloy

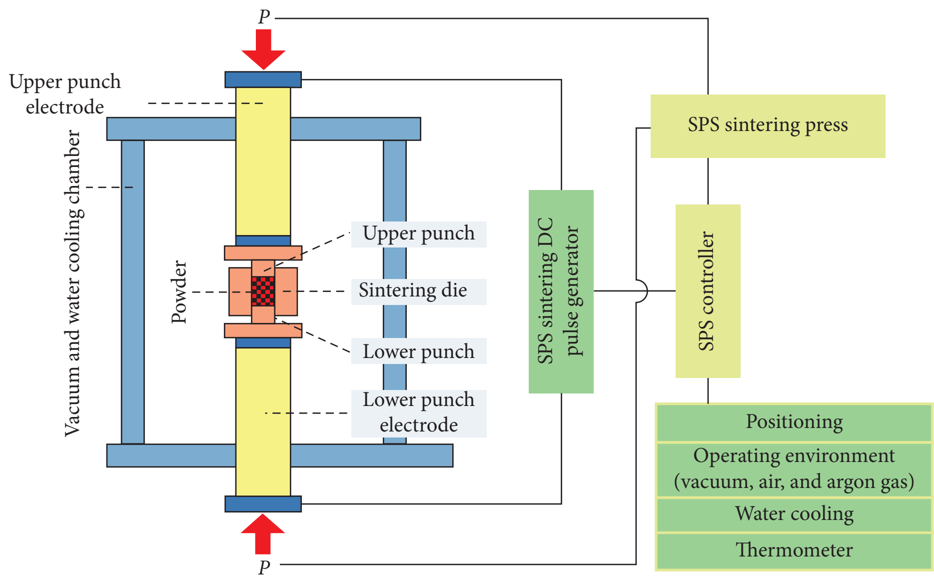

Figure 9: Typical spark plasma sintering (SPS) setup, as adopted from [87].

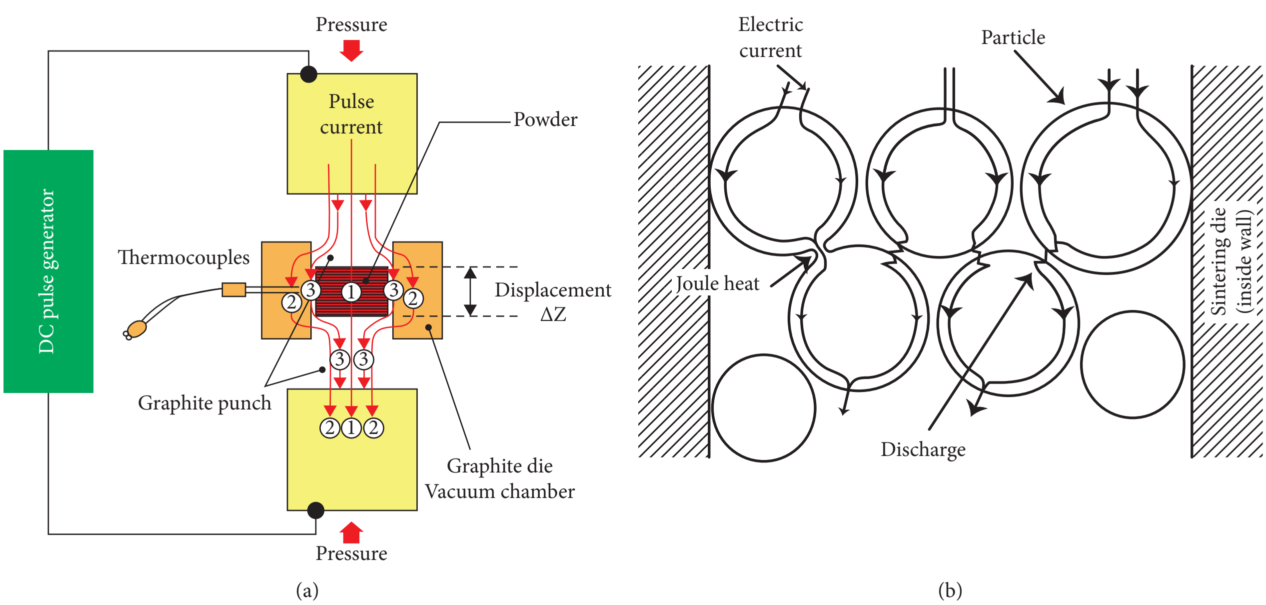

Figure 10: Pulse current flow through (a) the spark plasma sintering (SPS) machine and (b) the powder particles, as adopted from [87].

using elemental powders. From the study, although a lower pressure was applied to avoid the segregation of Al, maximum densification of the alloy was attained at higher temperatures up to 1573 K. Conversely, Wang et al. [91] reported that the application of higher pressure during SPS culminated in the imposition of larger sintering stresses at the contact areas of the powders. The large stresses led to the severe deformation and promoted mass transport of the particles resulting in good compaction of the TiAl alloy.

The applied current pulses and heating rate in the densification mechanisms of TiAl powders are deemed to affect the final microstructure of the alloy. High heating rates can result in near full densities of TiAl alloys, in a relatively short sintering time, which also lead to improved efficiency of the SPS process [92]. Furthermore, Zhang and coworkers [93] inferred that a high heating rate encourages grain refinement in TiAl alloys. The application of current pulses is well known from the literature to enhance mass transport through electron migration, generation of point defects, and improved defect mobility [94, 95]. At a microscopic scale with focus on the necks of the powder-powder interfaces, the applied current pulses have been shown besides being responsible for the Joule heating at the contact areas of the powders to culminate also in the particles indenting each other during densification [96]. The areas of contact are thus characterised by a recovery-recrystallisation mechanism, as depicted in Figure 11.

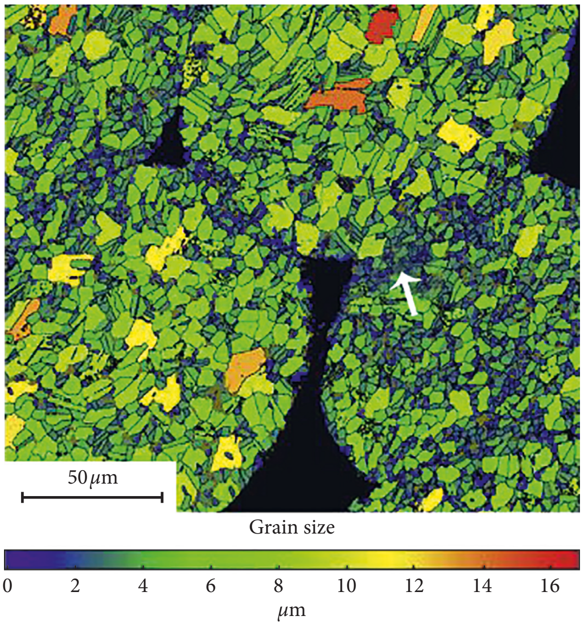

Figure 11: Size of the γ-grains mapped by EBSD between powder particles (densification at 1421 K). Grains are coloured in the function of their size (see colour scale) defined as the diameter of the circle of the same area. Small grains (in blue) are concentrated in the neck regions. The α_2 gains are coloured in olive green. The arrow indicates a concave interface for the particle at the middle right, indicating a strong plastic deformation of this particle, as adopted from [96].

Various investigations on the role of holding temperatures on the densification and grain sizes of the final microstructures of TiAl powders indicated that increasing the sintering temperature during the SPS process results in the strengthening of interparticle bonding and subsequent fabrication of denser alloys [92, 97–99]. Jabbar et al. [100] by using interrupted tests during the SPS process studied the effects of different sintering temperatures on the microstructural evolution of an equilibrated G4 powder alloy (Ti–47Al–1W–1Re–0.2Si at.%). The authors reported the initial microstructure of the powders had a dendritic morphology and a predominant metastable α-phase. However, their heating caused the transformation of the α- to the γ-phase with W and Re occupying the dendritic arms. At temperatures exceeding 1148 K , precipitations rich in W and Re of the B2 phase occurred. The densification process was thus attributed solely to plastic deformation.

Nevertheless, sintering at high temperatures is sometimes not recommended since it makes retaining ultrafine or nanostructures challenging [59].

In a nutshell, it is worth noting that SPS equipment varies and therefore caution should be taken in comparing sintering temperatures since different temperature measurements are employed, and none of them provides an accurate indication of the sample temperature.

The role of dwell time during the sintering process has been investigated by Wu et al. [101] as well. The authors concluded that prolonging holding time had little influence on the relative densities of the γ-TiAl alloy produced. However, increased holding time in the study resulted in significant improvement in the microhardness of the alloys. One of the underlying reasons for the use of SPS is to avoid grain growth in the final microstructure of alloys; thus, longer holding times are usually not encouraged.

7. Mechanical Properties

7.1. Dynamic Recrystallisation (DRX). As a structural material, TiAl alloys' mechanical properties are strongly dependent on the alloy composition, chemistry, microstructure, and test conditions such as temperature and strain rates. Plastic deformation of TiAl alloys mostly occurs in the γ-phase compared to the α_2-phase. Ordinary and superlattice dislocations, mechanical twinning, dynamic recovery, and recrystallisation mechanisms characterise the mode of deformation in TiAl alloys. In the c-direction of the tetragonal $L1_0$ lattice of the γ-phase, planes with Ti and Al atoms alternate. Therefore, ordinary dislocations with Burger vector $\mathbf{b}$ ($a_o/2 < 110]$) with non-c-components are anticipated to glide easily without altering the Ti and Al atoms at their respective positions in the lattice planes [102]. At temperatures below the brittle-to-ductile transition temperature (BDTT), the glide of ordinary $(1/2) < 110]\{111\}$ dislocations and mechanical twinning activated by the glide of Shockley dislocations along $(1/6) < 11\overline{2}]\{111\}$ are the predominant deformation mechanisms [103]. The elongation of ordinary dislocations along their screw orientation and their anchoring at various pinning points is observed in the γ-phase deformed at ambient temperature [104, 105]. The presence of frictional forces hindering dislocation mobility is responsible for the dislocations' elongation in their screw direction [104]. Additionally, the many dislocation pinning points are attributed to local chemical heterogeneities such as segregation of some interstitial oxygen atoms or Al_2O_3 precipitates [106].

Stacking fault energy (SFE) is also essential to deformation mechanisms of materials. SFE determines the interspacing of dissociated partial dislocations and thus influences the cross-slip properties of screw dislocations [103]. Materials with low SFE tend to demonstrate more mechanical twinning, whereby they possess an additional deformation mechanism [107]. TiAl alloys possess a much lower SFE compared to ordinary metals and alloys. Moreover, the smaller SFE of the γ-phase (60–90 m $(J\cdot m)^{-2}$) compared to the α_2-phase explains the occurrence of twinning in the γ-phase during deformation processes [108].

Of more interest in this section of the review are the dynamic recrystallisation and recovery mechanisms underlying deformation at elevated temperatures. However, for further insight into dislocation and mechanical twinning mechanisms as well as their interaction during deformation at either room or elevated temperatures, the following references are suggested to the reader [109–116].

Dynamic recrystallisation (DRX) is a softening process that can occur during high-temperature deformation of TiAl alloys. Some key features of DRX include the following [117, 118]:

(1) For DRX to occur, critical values of strain (associated with a critical dislocation density) and temperature (associated with a high enough mobility of grain boundaries) must be exceeded.

(2) DRX is characterised by the nucleation and growth of new grains from appropriate small regions. The newly nucleated grains often form at preexisting boundaries. The driving force for grain growth during DRX, i.e., total elastic strain energy of all dislocations in the deformed microstructure, is much higher than the driving force for normal grain growth (surface energy).

(3) The occurrence of DRX and formation of new dislocation-free grains are observed as sudden stress decreases in a stress-strain curve for a constant strain rate (CSR) test. As deformation advances, the dislocation density in the newly formed grains increases and the stress in the CSR test increases again. This can occur more than once and is depicted as stress fluctuations in the curve. In a constant stress creep experiment, this phenomenon produces strain rate peaks. For such fluctuations to be observed, the recrystallised volume fraction must be large enough.

(4) DRX occurs simultaneously with dynamic recovery, which does not necessarily culminate in the formation of new grains. Both processes are characterised by a specific kinetic and depending on the temperature, stress, and strain rate range of the experiment, either one of the two processes can dominate, or they can occur concurrently. Whether dynamic recrystallisation occurs or not at a given set of stress, temperature, and strain rate also depends on the material.

There are two types of DRX processes. They are continuous DRX (CDRX) and discontinuous DRX (DDRX) [118]. The DDRX takes place in materials with relatively low stacking fault energies and is associated with a bulging operating mechanism. With respect to CDRX, newly formed low-angle grain boundaries gradually transform into high-angle grain boundaries and eventually turn into recrystallised grains during straining [119]. Two primary processes govern CDRX. They are progressive new grain rotation and geometric dynamic recrystallisation, as depicted in Figure 12. The CDRX usually transpires in materials with high stacking fault energies [119].

Numerous studies have reported on DRX during hot deformation of TiAl alloys. Rudolf et al. [102] attributed the overall strain compatibility of their Ti–47Al–2Mn–2Nb +0.8 vol.% TiB_2 alloy to dynamic recrystallisation and not superdislocation. The authors credited the advent of the minimum creep rate in counteracting work hardening to dynamic recrystallisation. The nucleation and growth of new grains annihilate high dislocation density regions. Dislocations can be generated within the new grains, which allow for further plastic deformation. Furthermore, the new grains may nucleate and grow in crystallographic directions, which favour dislocation plasticity. So, wherever strain compatibility is required, dynamic recrystallisation provides new grains, which can deform in directions, which are needed for homogeneous macroscopic deformation. Also, during hot deformation, microstructure restoration is ascribed mainly to dynamic recrystallisation and continuous recrystallisation mechanisms commencing even at lower strain rates [121]. DRX behaviour closely relates to microstructures, and microstructures influence the mechanical properties of TiAl alloys. DRX has been reported to refine the microstructures of TiAl alloys [34]. Grain refinement over the years is deemed an effective means in improving the performance of TiAl alloys. Additionally, the formation of certain phases such as the β-phase, silicide, and h-type carbides enhances DRX behaviour [34]. Al contents in TiAl alloys, on the other hand, affect DRX kinetics. Imayev et al. [122] indicated that TiAl alloys with nearly stoichiometric compositions exhibit a fast DRX kinetics while recrystallisation kinetics decreases for lower or higher Al contents. Consistent with findings by Cheng et al. [123], DRX kinetics in Al-lean TNB alloys are also slow. The occurrence of DRX in the boundaries of lamellar colonies and also in the boundaries of dynamically recrystallised grains during uniaxial hot compression tests under various deformation conditions of a TNM alloy have been reported by Xiang and colleagues [124]. The increasing DRX processes during deformation led not only to the decomposition of the lamellar structure but also to the precipitation of completely dynamically crystallised equiaxed β-phase. The β-phase preferentially nucleated at the boundaries of the remnant α_2 laths and the γ laths. Again, several research studies have hinted on the preferential nucleation of DRX at the triple colony boundaries of the lamellar structure [125–127]. This is premised on deformation being the largest at the triple boundaries. Figure 13 summarises the DRX process in the α_2/γ lamellar colonies. Hao et al. [128] elaborated from their study with respect to Figure 13 that at the early stage of deformation, nucleation and annihilation of numerous nanotwins at adjacent lamellar interfaces occur. Concurrently, large amounts of dislocations generate from the γ lamellas, as depicted in Figure 13(b). With increase in strain, plenty of dislocations pile up at the twin boundaries and lamellar interfaces, as shown in Figure 13(c). As deformation continues, many dislocations are absorbed, leading to the formation of subgrain boundaries. The γ lamellas are then divided into many subgrains, as shown in Figure 13(d). With increased misorientation between adjacent subgrains, the subgrain boundaries transform into refined grain boundaries and eventually accomplish dynamic recrystallisation, as illustrated in Figure 13(e).

7.1.1. DRX Models. The dynamic material model (DMM) technique proposed by Prasad et al. [129], over the years, has been used to analyse quantitatively hot deformation of materials. A good example is the use of processing maps. Processing maps are contour plots of the variation of efficiency values against deformation temperature and strain rate under a given strain [130]. The efficacy of processing maps to attain optimum processing domains of metals and

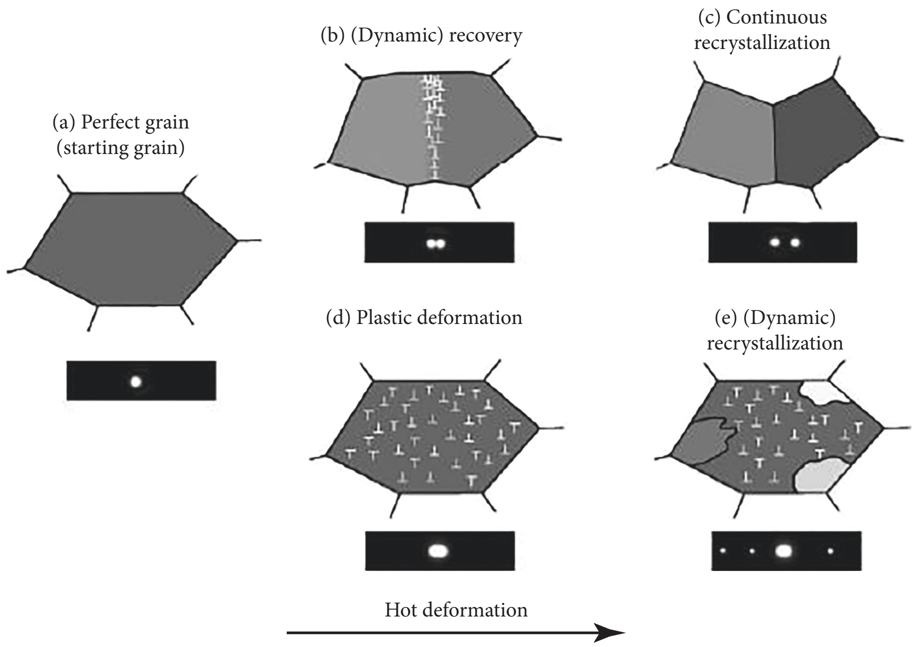

FIGURE 12: Schematic model that illustrates the development of reflection spots dependent on the different processes that might occur during hot deformation of TiAl alloys. Starting with a perfect grain, plastic deformation increases from left to right. The development of the corresponding reflection spot is indicated below. In (a), a sharp reflection spot of a perfect grain is visible. Images (b) and (c) show how dislocations are introduced by plastic deformation which forms a subgrain boundary in (b) through dynamic recovery processes and eventually a high-angle grain boundary in (c). In contrast to this, images (d) and (e) show a case where the defect density increases until the onset of recrystallisation which is illustrated by the nucleation of new grains (adopted from [120]).

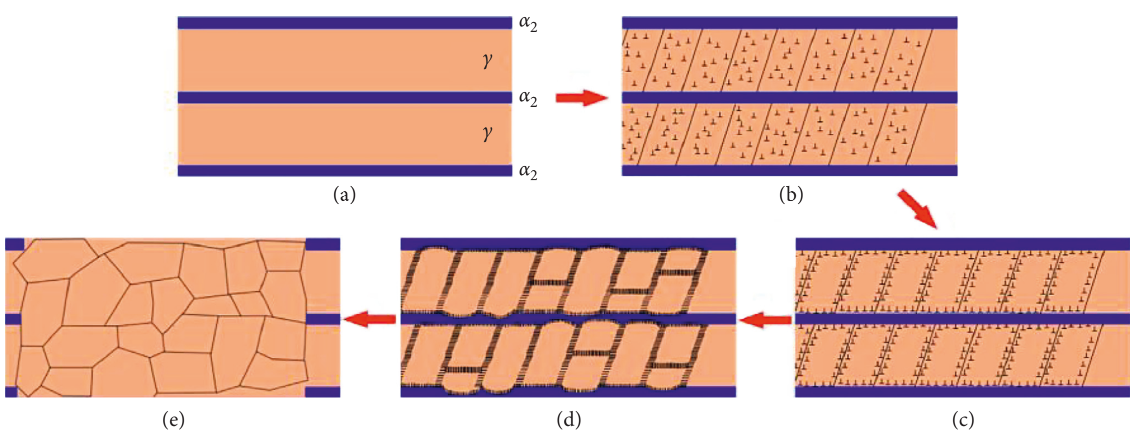

FIGURE 13: Schematic illustration showing the DRX process in the α_2/γ lamellar colonies (adopted from [128]).

alloys and serve as guidance for practical plastic forming have been reported [44, 131–135]. The reader is referred to [136–140] for information on the fundamentals and details of processing maps. DRX occurrence has been correlated to the stable domains in processing maps [141, 142]. Essential to microstructural evolution, the event of DRX is considered the main power dissipation mechanism during hot deformation. DRX behaviour is beneficial not only to refining grain size, enhancing structural homogeneity, or improving production mechanical properties from processes such as forging but also is an efficient mechanism to attain work hardening rate and flow stress at low levels [130].

A mathematical model based on the Avrami equation has also been used to investigate DRX kinetics of TiAl alloys during hot compression testing [143, 144]. As well known, DRX of a material will start when the critical strain is exceeded. The degree of DRX subject to different processing parameters is described by its volume fraction [143]. From the theory of DRX dynamics, the relationship between DRX volume fraction and strain (ε) can be expressed by the Avrami equation as [143, 145]

$$X_{\mathrm{DRX}} = 1 - e^{\left(-k\left[\left(\varepsilon-\varepsilon_c\right)/\varepsilon_p\right]^n\right)}, \quad (1)$$

where X_{DRX} is the volume fraction of DRX grains, k is a material constant, ε_c and ε_p are critical and peak strain, respectively, and n is the Avrami constant.

From equating X_{DRX} to flow stress, we get

$$X_{DRX} = \frac{(\sigma_p - \sigma)}{(\sigma_p - \sigma_{ss})}, \quad (2)$$

where σ_{ss} denotes steady-state stress; and by using regression analysis, the average k and n values for the DRX kinetic model can be determined from equations (1) and (2) [143].

In summary, from the plot of X_{DRX} vs ε involving the DRX kinetic model at various deformation temperatures and strain rates, the influence of hot deformation parameters on DRX behaviour and volume fraction can be assessed. Thus, an increase in strain rate and decrease in deformation temperature result in a decrease in DRX volume fraction and grain size. This is in good agreement with other reported studies [127, 146, 147]. In general, the occurrence of DRX is mainly due to dislocation glide or dislocation climb. Deformation at high temperature enhances the diffusion of atoms, cross-slip dislocation, and migration of grain boundaries, which is beneficial to nucleation and nucleus growth of DRX [148].

Other models used to analyse DRX behaviours during hot deformation of TiAl alloys are the constitutive models. Some include the Arrhenius-type constitutive model [119, 142, 149] and experimental models such as Sellars–McTegart and Hensel–Spittel models [121].

8. Oxidation Resistance

8.1. Overview and Formation of Oxides. The oxidation of metal (M) in pure oxygen forms an oxide (M_aO_b) according to the reaction:

$$a \cdot M + \frac{b}{2}O_2 \longrightarrow M_aO_b. \quad (3)$$

However, in applications, the presence of other parameters from the service environment complicates the oxidation process. The formation of surface oxides separates the metal surface from the environment. The formed surface oxides serve as a barrier layer which retards further oxidation reaction and decreases metal consumption. An underlying feature desired for high-temperature materials is their capability to form protective surface oxides able to resist service conditions such as hot gases and offer long-term protection during use.

The formation of surface oxides on alloys, in general, can be fundamentally described in four stages, as illustrated in Figure 14. They include, foremost, oxygen adsorption at the surface, nucleation of the oxides, and lateral growth of the nuclei, which subsequently forms a compact oxide scale [150]. For a beneficial effect, the formed surface oxides must be thermodynamically stable in the service environment, must adhere to the alloy surface, must be thermo-mechanically compatible with the metal, exhibit a low growth rate and capable of self-healing [151].

Figure 15 shows the oxidation zone at the surface of titanium-based alloys with varying Al content exposed to identical oxidation conditions. Although oxide formation can be complex, the figure provides insights into the principal differences in oxide arrangements.

A well-noticed advantage of γ-TiAl-based alloys during service is their resistance to oxidation in temperature ranges between 823 and 1123 K. The corrosion reaction products formed on the surface of these alloys are influenced by the alloy chemistry, exposure temperature, and duration, and the oxidising atmosphere. The primary oxides associated with TiAl-based alloys as depicted in Figure 15 include rutile (TiO_2), the low-oxidation temperature corundum phase of alumina (α-Al_2O_3), and a heterogeneous mixture of the two oxides ($TiO_2 + Al_2O_3$). Despite the competition between Al-O and Ti-O bonds at the adsorbed surface of TiAl-based alloys, the high tendency of formation of TiO_2 is due to the preference of oxygen atoms to Ti-rich areas [151]. As a continuous and porous TiO_2 is formed at the outermost surface, Al becomes locally enriched underneath the TiO_2 leading to Al-O bonds growing stronger relative to Ti-O bonds promoting the formation of Al_2O_3 oxides [153]. Also, this accounts for the mixed oxide zone of TiO_2 and Al_2O_3 at the subsurface [154].

Furthermore, TiO_2 is built on the oxide outermost parts rather than Al_2O_3 because of the fast-growing kinetics of TiO_2 compared to Al_2O_3 [155, 156]. Therefore, due to the slower diffusion of Al, a rich Al_2O_3 layer is generated under the TiO_2. TiO_2 is characterised as less dense and off-stoichiometric n-type oxide. It is flawed with oxygen vacancies which tend to be paths for fast diffusion of oxygen, making them unprotective and significantly limiting the oxidation resistance of TiAl-based alloys [155, 156].

From Figure 15, the addition of Al decreases the width of the oxygen-affected zone. The incorporation of more Al results in a reduction of the oxide thickness, which means an improvement in oxidation resistance of the oxide [152, 157]. The Al_2O_3 formation is greatly desired because of its inherent protective nature as a surface oxide. This is because of attributes exhibited such as excellent compactness, good adhesion, and low growth rate [157]. TiO_2 and Al_2O_3 make up the outermost oxides formed on the surface of TiAl-based alloys due to their outward growing nature while a mixture of the two oxides ($TiO_2 + Al_2O_3$) grows inward forming inner oxides [158].

Furthermore, the influence of alloy microstructures on the formation of surface oxides has been contradicting. For instance, in a reported comparison study of near-α alloys with lamellar and bimodal microstructures, improved oxidation resistance was observed from the alloy with the lamellar structure [152]. Conversely, Yamaguchi et al. [11] suggested that the oxidation resistance of TiAl alloys is independent of the microstructure of the compositions.

8.2. Influence of Ternary Elements on Oxidation Resistance. Again, one element that has received wide attention in enhancing the oxidation performance of TiAl alloys is Nb [159–164]. The efficacy of Nb in improving oxidation performance is ascribed to the doping effect concept. The vacancies in the rutile lead to internal oxidation by promoting

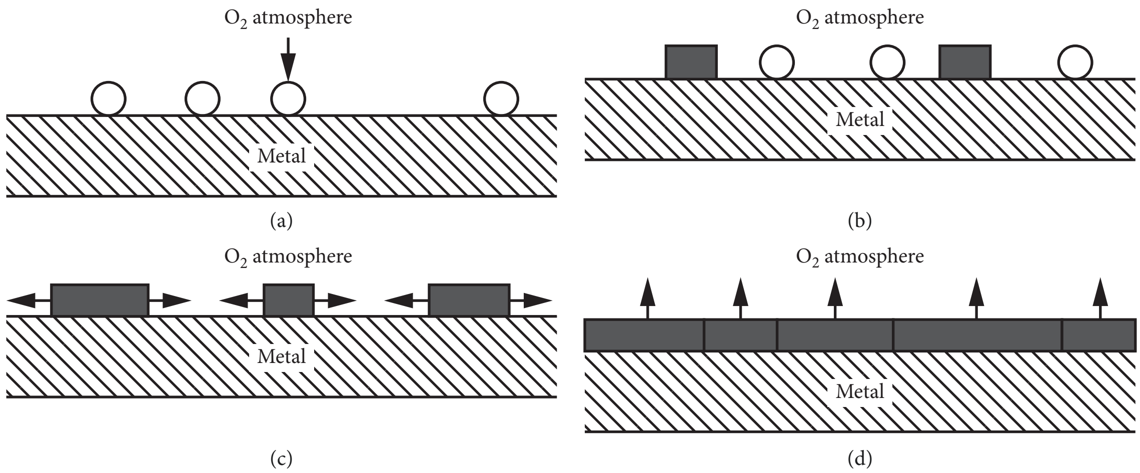

FIGURE 14: Model of oxide scale formation on the pure metal surface. (a) Oxygen absorption at the surface; (b) formation of nuclei; (c) lateral growth of nuclei; (d) the growth of the oxide scale [152].

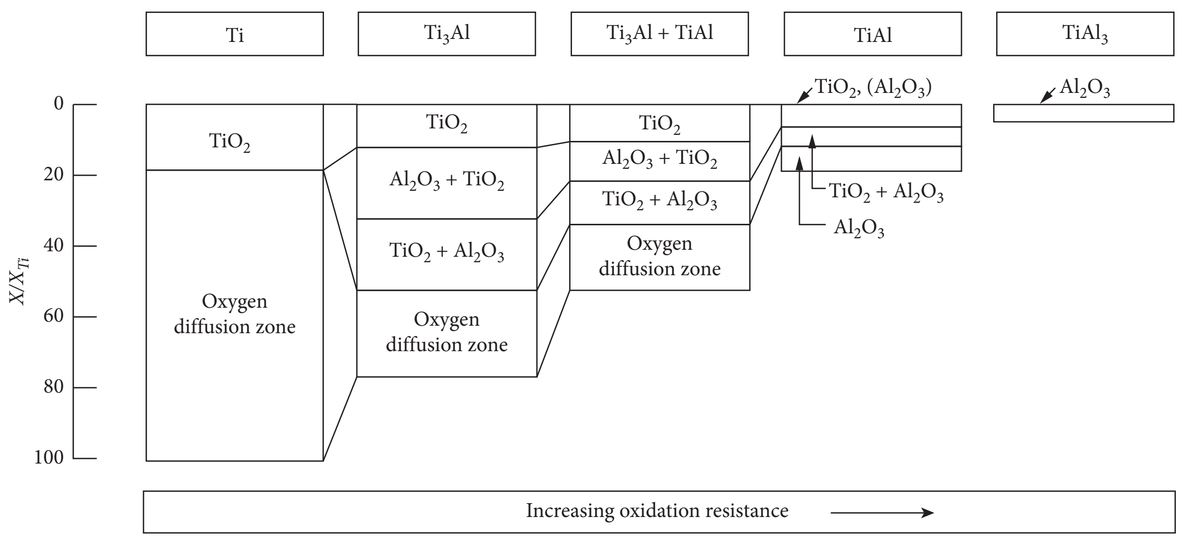

FIGURE 15: Schematic representation of oxide scales and oxygen diffusion zones of titanium-based alloys [151].

the inward diffusion of oxygen. Hence, the addition of a dopant elements such as Nb with a valence electron (+5) higher than that of Ti (+4) culminates in the decrease of defect concentration (or oxygen vacancy concentration) due to attaining electroneutrality in the oxide. This subsequently promotes the activities of Al relative to Ti, slowing the growth of TiO_2 and thus favouring the establishment of a denser, continuous, and adherent Al_2O_3 layer which acts as a protective barrier [165]. Furthermore, the development of TiN and Ti_2AlN oxides at the oxide/substrate interface serves as an excellent diffusion barrier preventing the diffusion of oxygen ions into the substrate. The presence of Nb tends to stabilise the oxide, minimise its transformation into rutile, and decrease the oxidation rate of the TiAl alloy [166].

An equal replacement of Nb is the use of Ta. Concerning their positions on the periodic table, the chemical behaviours of both elements are alike. Ta as an element is naturally known for its excellent resistance to oxidation. Additionally, as a marked advantage, Ta has a high melting temperature, thus presenting the opportunity of increasing the service temperature of TiAl alloys. Despite this knowledge, there is very limited research with contradicting findings on the influence of Ta on the oxidation resistance of TiAl alloys. Shida and Anada [167] concluded in their study that Ta additions played no role in the oxidation resistance of Ti-48.6Al (at.%) alloy. Other studies [168–170] reported that Ta additions were not significantly effective compared to Nb against oxidation. In contention, studies by Popela et al. [171] on Ti-46Al-8Ta (at.%) alloy which was compared to Ti-46Al-8Nb (at.%) reported that the specific weight reduction of the Ti-46Al-8Ta (at.%) alloy was two orders lower compared to the Ti-46Al-8Nb (at.%) alloy. Furthermore, it was concluded that at temperatures of 1273 K and higher, the effect of Ta additions on oxidation resistivity was better than the Nb-containing alloy because of its ability to form a significantly denser, adherent, and protective oxides. Similarly, in a comparison study of Ti-44.8Al-6.6Ta and Ti-45.2Al-7.2Nb (at.%) investigated by Vojtěch et al. [172], the positive influence of Ta at 1273 K was attributed to the more stable and adherent oxides formed and the lower tendency of oxides spallation during cyclic oxidation. In summary, Ta tends to reduce the solubility of oxygen in TiAl alloys, therefore suppressing rutile (TiO_2) formation and growth [173, 174].

The presence of Cr in TiAl during oxidation also takes the role of a doping element which restricts the permeation of oxygen and promotes preferential oxidation of Al [175]. At elevated temperatures ($T > 673$ K), Cr forms Cr_2O_3. Cr_2O_3 has a corundum structure like Al_2O_3 and is also a protective oxide owing to its parabolic growth mechanisms [176]. Cr in TiAl alloys has been suggested to enhance adhesion of oxide mixtures of Al_2O_3 and TiO_2 due to its solubility in Al_2O_3 and compatibility with TiO_2 [175]. On the other hand, the potency of Cr in positively influencing oxidation resistance of TiAl alloys is largely dependent on its concentration. Cr additions higher than 8 at.% have beneficial effects in TiAl alloys, whereas concentrations lower than 4 at.% are detrimental [177].

Also, W and Mo improve oxidation resistance by forming W- or Mo-+enriched β-Ti phases such as Ti_2AlMo and/or δ-Ti phase at the metal side of the oxide/metal interface [178]. Oxygen solubility in the formed layer is low, whereas Al diffusion is fast [178]. This drives not only the supply of Al into the oxide scale but also leads to the formation of Al_2O_3 at the oxide/metal interface [167].

The addition of Y in the right amount influences the oxidation resistance of TiAl alloys. The incorporation of Y significantly improves long-time oxidation resistance by retarding rutile formation, favouring Al_2O_3 formation and growth, and also strengthening the spallation resistance of formed scales [179]. During oxidation, Y promotes the generation of a Y-rich layer at the immediate surface of TiAl alloys. Y has a strong affinity to oxygen during high-temperature oxidation and hence forms Y_2O_3 oxide and (Y, Al) O-type oxides [180]. While formed Al_2O_3 acts as diffusion barriers impeding oxygen ingress, the inner (Y, Al) O-type oxides tend to reduce thermal stress by modifying the oxide layer's grain structure. Hence, the residual stress between the oxide scale and substrate may be removed [181]. The beneficial effect of Y on the scale spallation of TiAl alloys is attributed to proposed mechanisms such as [181–183]

(1) The reactive-element-oxide particles encourage mechanical keying of the oxide scale on the substrate
(2) The reactive elements tend to serve as vacancy sink sites resulting in the suppression of vacancy coalescence at the alloy-oxide interface for void formation
(3) The segregation of Y at the oxide grain boundaries blocks diffusion paths and thus decreases growth stress in the scale
(4) The formation of a fine-grain layer structure improves the plasticity of the oxide scale

Another concept used in improving the oxidation resistance of TiAl alloys includes the incorporation of halogens (F, Cl, Br, and I) termed as the halogen effect. The addition of halogens has been investigated and concluded to support selective Al transport and improve adhesion between the formed Al_2O_3 scale and the metal surface. For detailed information, the reader is referred to the following references [184–189].

9. Conclusion

Titanium aluminide- (TiAl-) based alloys have gained immense recognition as a new group of weight-saving materials. Their properties, to some extent, better the shortcomings of conventional titanium alloys at higher temperatures.

The effectiveness of the powder metallurgy route of manufacturing TiAl alloys, in recent years, has been promising. The combined use of high-energy mechanical milling and spark plasma sintering increases the tendency of attaining ultrafine and homogeneous microstructures at a cheaper cost. The PM route, together with microalloying, enhances specific properties despite the tradeoff of others. The addition of niobium (Nb) has stood out compared to other elements in achieving the right balance of properties at both ambient and elevated temperatures.

In summary, the competent usage of TiAl-based alloys as structural engineering materials rests on the application of the most effective tailored microstructures attained through controlled processing and appropriate alloy modifications that can promote and stabilise new microstructures. Thus, there is the need to understand the fundamentals of alloy design, processing, characterisation of the microstructures, microstructure and property relationship, behaviour or performance of these new alloys as well as the influence of the environment on these properties during service.

Conflicts of Interest

The authors declare that there are no conflicts of interest regarding the publication of this paper.

References

[1] F. H. Froes, C. Suryanarayana, and D. Eliezer, "Synthesis, properties and applications of titanium aluminides," *Journal of Materials Science*, vol. 27, no. 19, pp. 5113–5140, 1992.
[2] A. Lasalmonie, "Intermetallics: why is it so difficult to introduce them in gas turbine engines?," *Intermetallics*, vol. 14, no. 10-11, pp. 1123–1129, 2006.
[3] F. Appel, J. D. H. Paul, and M. Oehring, *Gamma Titanium Aluminide Alloys: Science and Technology*, John Wiley & Sons, Hoboken, NJ, USA, 2011.
[4] H. Clemens and S. Mayer, "Intermetallic titanium aluminides in aerospace applications–processing, microstructure and properties," *Materials at High Temperatures*, vol. 33, no. 4-5, pp. 560–570, 2016.
[5] S. Mayer, P. Erdely, F. D. Fischer et al., "Intermetallic β-solidifying γ-TiAl based alloys—from fundamental research to application," *Advanced Engineering Materials*, vol. 19, no. 4, Article ID 1600735, 2017.
[6] B. Bewlay, S. Nag, A. Suzuki, and M. Weimer, "TiAl alloys in commercial aircraft engines," *Materials at High Temperatures*, vol. 33, no. 4-5, pp. 549–559, 2016.

[7] T. Tetsui, "Manufacturing technology for gamma-TiAl alloy in current and future applications," *Rare Metals*, vol. 30, no. 1, pp. 294–299, 2011.
[8] E. A. Loria, "Quo vadis gamma titanium aluminide," *Intermetallics*, vol. 9, no. 12, pp. 997–1001, 2001.
[9] S. Djanarthany, J.-C. Viala, and J. Bouix, "An overview of monolithic titanium aluminides based on Ti_3Al and TiAl," *Materials Chemistry and Physics*, vol. 72, no. 3, pp. 301–319, 2001.
[10] L. Lü and M. O. Lai, *Mechanical Alloying*, Springer Science & Business Media, New York, NY, USA, 2013.
[11] M. Yamaguchi, H. Inui, and K. Ito, "High-temperature structural intermetallics," *Acta Materialia*, vol. 48, no. 1, pp. 307–322, 2000.
[12] L. Lü and M. O. Lai, "Introduction to mechanical alloying," in *Mechanical Alloying*, pp. 1–9, Springer, Boston, MA, USA, 1998.
[13] F. Appel, H. Clemens, and F. D. Fischer, "Modeling concepts for intermetallic titanium aluminides," *Progress in Materials Science*, vol. 81, pp. 55–124, 2016.
[14] F. Kong, Y. Chen, and F. Yang, "Effect of heat treatment on microstructures and tensile properties of as-forged Ti-45Al-5Nb-0.3Y alloy," *Intermetallics*, vol. 19, no. 2, pp. 212–216, 2011.
[15] K. Kothari, R. Radhakrishnan, and N. M. Wereley, "Advances in gamma titanium aluminides and their manufacturing techniques," *Progress in Aerospace Sciences*, vol. 55, pp. 1–16, 2012.
[16] H. Clemens and S. Mayer, "Design, processing, microstructure, properties, and applications of advanced intermetallic TiAl alloys," *Advanced Engineering Materials*, vol. 15, no. 4, pp. 191–215, 2013.
[17] X. Wu, "Review of alloy and process development of TiAl alloys," *Intermetallics*, vol. 14, no. 10-11, pp. 1114–1122, 2006.
[18] J. Chrapoński, W. Szkliniarz, A. Kościelna, and B. Serek, "Microstructure and chemical composition of phases in Ti–48Al–2Cr–2Nb intermetallic alloy," *Materials Chemistry and Physics*, vol. 81, no. 2-3, pp. 438–442, 2003.
[19] H. Clemens, A. Bartels, S. Bystrzanowski et al., "Grain refinement in γ-TiAl-based alloys by solid state phase transformations," *Intermetallics*, vol. 14, no. 12, pp. 1380–1385, 2006.
[20] H. Saage, A. Huang, D. Hu, M. Loretto, and X. Wu, "Microstructures and tensile properties of massively transformed and aged Ti46Al8Nb and Ti46Al8Ta alloys," *Intermetallics*, vol. 17, no. 1-2, pp. 32–38, 2009.
[21] D. Hu, A. J. Huang, and X. Wu, "On the massive phase transformation regime in TiAl alloys: the alloying effect on massive/lamellar competition," *Intermetallics*, vol. 15, no. 3, pp. 327–332, 2007.
[22] S. Banumathy, N. Sruti Neelam, V. Chandravanshi, A. Bhattacharjee, and K. R. Ravi, "The Effect of Nb addition on microstructure, oxidation behavior and strength of some γ-TiAl alloys," *Materials Today: Proceedings*, vol. 5, no. 2, pp. 5514–5520, 2018.
[23] T. Klein, B. Rashkova, D. Holec, H. Clemens, and S. Mayer, "Silicon distribution and silicide precipitation during annealing in an advanced multi-phase γ-TiAl based alloy," *Acta Materialia*, vol. 110, pp. 236–245, 2016.
[24] S.-L. Xiao, L.-J. Xu, Y.-Y. Chen, and H.-B. Yu, "Microstructure and mechanical properties of TiAl-based alloy prepared by double mechanical milling and spark plasma sintering," *Transactions of Nonferrous Metals Society of China*, vol. 22, no. 5, pp. 1086–1091, 2012.
[25] D. Hu, J. F. Mei, M. Wickins, and R. A. Harding, "Microstructure and tensile properties of investment cast Ti-46Al-8Nb-1B alloy," *Scripta Materialia*, vol. 47, no. 4, pp. 273–278, 2002.
[26] Y. Liu, H. Li, S. Wang, and H. Ye, "Nb effects on the structural and mechanical properties of TiAl alloy: density-functional theory study," *Journal of Materials Research*, vol. 24, no. 10, pp. 3165–3173, 2009.
[27] Y.-W. Kim and D. M. Dimiduk, "Progress in the understanding of gamma titanium aluminides," *JOM*, vol. 43, no. 8, pp. 40–47, 1991.
[28] G. Chen, X. Xu, Z. Teng, Y. Wang, and J. Lin, "Microsegregation in high Nb containing TiAl alloy ingots beyond laboratory scale," *Intermetallics*, vol. 15, no. 5-6, pp. 625–631, 2007.
[29] H. Jabbar, J.-P. Monchoux, F. Houdellier et al., "Microstructure and mechanical properties of high niobium containing TiAl alloys elaborated by spark plasma sintering," *Intermetallics*, vol. 18, no. 12, pp. 2312–2321, 2010.
[30] H. Jabbar, J.-P. Monchoux, M. Thomas, F. Pyczak, and A. Couret, "Improvement of the creep properties of TiAl alloys densified by spark plasma sintering," *Intermetallics*, vol. 46, pp. 1–3, 2014.
[31] E. Hamzah, M. Kanniah, and M. Harun, "Effect of beta phase on room to high temperature mechanical properties of as-cast gamma titanium aluminide," *Mechanics of Advanced Materials and Structures*, vol. 16, no. 5, pp. 384–389, 2009.
[32] C. Kenel and C. Leinenbach, "Influence of Nb and Mo on microstructure formation of rapidly solidified ternary Ti–Al-(Nb, Mo) alloys," *Intermetallics*, vol. 69, pp. 82–89, 2016.
[33] M. Kastenhuber, B. Rashkova, H. Clemens, and S. Mayer, "Enhancement of creep properties and microstructural stability of intermetallic β-solidifying γ-TiAl based alloys," *Intermetallics*, vol. 63, pp. 19–26, 2015.
[34] E. Schwaighofer, H. Clemens, J. Lindemann, A. Stark, and S. Mayer, "Hot-working behavior of an advanced intermetallic multi-phase γ-TiAl based alloy," *Materials Science and Engineering: A*, vol. 614, pp. 297–310, 2014.
[35] T. Klein, L. Usategui, B. Rashkova et al., "Mechanical behavior and related microstructural aspects of a nano-lamellar TiAl alloy at elevated temperatures," *Acta Materialia*, vol. 128, pp. 440–450, 2017.
[36] M. Kastenhuber, T. Klein, B. Rashkova, I. Weißensteiner, H. Clemens, and S. Mayer, "Phase transformations in a β-solidifying γ-TiAl based alloy during rapid solidification," *Intermetallics*, vol. 91, pp. 100–109, 2017.
[37] L. Germann, D. Banerjee, J. Y. Guédou, and J.-L. Strudel, "Effect of composition on the mechanical properties of newly developed Ti_2AlNb-based titanium aluminide," *Intermetallics*, vol. 13, no. 9, pp. 920–924, 2005.
[38] G. E. Fuchs, "High temperature alloys," in *Kirk-Othmer Encyclopedia of Chemical Technology*, pp. 469–532, John Wiley & Sons, Inc, New York, NY, USA, 2005.
[39] T. Kawabata, T. Tamura, and O. Izumi, "Effect of Ti/Al ratio and Cr, Nb, and Hf additions on material factors and mechanical properties in TiAl," *Metallurgical Transactions A*, vol. 24, no. 1, pp. 141–150, 1993.
[40] Q. Wang, H. Ding, H. Zhang, R. Chen, J. Guo, and H. Fu, "Influence of Mn addition on the microstructure and mechanical properties of a directionally solidified γ-TiAl alloy," *Materials Characterization*, vol. 137, pp. 133–141, 2018.
[41] S.-C. Huang and E. L. Hall, "The effects of Cr additions to binary TiAl-base alloys," *Metallurgical Transactions A*, vol. 22, no. 11, pp. 2619–2627, 1991.

[42] M. Takeyama and S. Kobayashi, "Physical metallurgy for wrought gamma titanium aluminides," *Intermetallics*, vol. 13, no. 9, pp. 993–999, 2005.

[43] Z. W. Huang, "Thermal stability of Ti-44Al-4Nb-4Hf-0.2Si-1B alloy," *Intermetallics*, vol. 37, pp. 11–21, 2013.

[44] V. Singh, C. Mondal, A. Kumar, P. P. Bhattacharjee, and P. Ghosal, "High temperature compressive flow behavior and associated microstructural development in a β-stabilized high Nb-containing γ-TiAl based alloy," *Journal of Alloys and Compounds*, vol. 788, pp. 573–585, 2019.

[45] E. Schwaighofer, B. Rashkova, H. Clemens, A. Stark, and S. Mayer, "Effect of carbon addition on solidification behavior, phase evolution and creep properties of an intermetallic β-stabilized γ-TiAl based alloy," *Intermetallics*, vol. 46, pp. 173–184, 2014.

[46] T. Klein, M. Schachermayer, F. Mendez-Martin et al., "Carbon distribution in multi-phase γ-TiAl based alloys and its influence on mechanical properties and phase formation," *Acta Materialia*, vol. 94, pp. 205–213, 2015.

[47] U. Hecht, V. Witusiewicz, A. Drevermann, and J. Zollinger, "Grain refinement by low boron additions in niobium-rich TiAl-based alloys," *Intermetallics*, vol. 16, no. 8, pp. 969–978, 2008.

[48] Z. G. Liu, X. Wang, X. P. Wang, C. J. Zhang, L. H. Chai, and Y. Y Chen, "Microstructural investigation of a rapidly solidified Ti–Zr–Fe–Si–Sn–Nb alloy," *Journal of Alloys and Compounds*, vol. 504, no. S1, pp. S480–S482, 2010.

[49] T. T. Cheng, M. R. Willis, and I. P. Jones, "Effects of major alloying additions on the microstructure and mechanical properties of γ-TiAl," *Intermetallics*, vol. 7, no. 1, pp. 89–99, 1999.

[50] J. Lapin, L. Ondrúš, and O. Bajana, "Effect of Al_2O_3 particles on mechanical properties of directionally solidified intermetallic Ti–46Al–2W–0.5 Si alloy," *Materials Science and Engineering A*, vol. 360, no. 1-2, pp. 85–95, 2003.

[51] T. Noda, M. Okabe, S. Isobe, and M. Sayashi, "Silicide precipitation strengthened TiAl," *Materials Science and Engineering: A*, vol. 192-193, pp. 774–779, 1995.

[52] Y.-W. Kim and S.-L. Kim, "Effects of microstructure and C and Si additions on elevated temperature creep and fatigue of gamma TiAl alloys," *Intermetallics*, vol. 53, pp. 92–101, 2014.

[53] X.-W. Du, J. N. Wang, and J. Zhu, "The influence of Si alloying on the crept microstructure and property of a TiAl alloy prepared by powder metallurgy," *Intermetallics*, vol. 9, no. 9, pp. 745–753, 2001.

[54] S. Naka, "Advanced titanium-based alloys," *Current Opinion in Solid State and Materials Science*, vol. 1, no. 3, pp. 333–339, 1996.

[55] H. Zhong, Y. Yang, J. Li et al., "Influence of oxygen on microstructure and phase transformation in high Nb containing TiAl alloys," *Materials Letters*, vol. 83, pp. 198–201, 2012.

[56] W. Lefebvre, A. Loiseau, and A. Menand, "Oxygen induced chemical ordering and ultrafine lamellar structure formation in a Ti-48 at.% Al alloy," *MRS Online Proceedings Library Archive*, vol. 753, 2002.

[57] A. Menand, A. Huguet, and A. Nérac-Partaix, "Interstitial solubility in γ and α_2 phases of TiAl-based alloys," *Acta Materialia*, vol. 44, no. 12, pp. 4729–4737, 1996.

[58] H. Hashimoto, T. Abe, and Z.-M. Sun, "Nitrogen-induced powder formation of titanium aluminides during mechanical alloying," *Intermetallics*, vol. 8, no. 7, pp. 721–728, 2000.

[59] Y. Liu and W. Liu, "Mechanical alloying and spark plasma sintering of the intermetallic compound $Ti_{50}Al_{50}$," *Journal of Alloys and Compounds*, vol. 440, no. 1-2, pp. 154–157, 2007.

[60] P. Bhattacharya, P. Bellon, R. S. Averback, and S. J. Hales, "Nanocrystalline TiAl powders synthesized by high-energy ball milling: effects of milling parameters on yield and contamination," *Journal of Alloys and Compounds*, vol. 368, no. 1-2, pp. 187–196, 2004.

[61] Z. W. Li, W. Gao, D. L. Zhang, and Z. H. Cai, "High temperature oxidation behaviour of a TiAl–Al_2O_3 intermetallic matrix composite," *Corrosion Science*, vol. 46, no. 8, pp. 1997–2007, 2004.

[62] A. Rahmel, M. Schütze, and W. J. Quadakkers, "Fundamentals of TiAl oxidation—a critical review," *Materials and Corrosion*, vol. 46, no. 5, pp. 271–285, 1995.

[63] T. Kawabata, T. Abumiya, and O. Izumi, "Effect of oxygen addition on mechanical properties of TiAl at 293–1273 K," *Acta Metallurgica et Materialia*, vol. 40, no. 10, pp. 2557–2567, 1992.

[64] J. J. Valencia, C. McCullough, C. G. Levi, and R. Mehrabian, "Solidification microstructure of supercooled Ti-Al alloys containing intermetallic phases," *Acta Metallurgica*, vol. 37, no. 9, pp. 2517–2530, 1989.

[65] K. Uenishi, T. Matsubara, M. Kambara, and K. Kobayashi, "Nanostructured titanium-aluminides and their composites formed by combustion synthesis of mechanically alloyed powders," *Scripta Materialia*, vol. 44, no. 8-9, pp. 2093–2097, 2001.

[66] C. Suryanarayana, "Mechanical alloying and milling," *Progress in Materials Science*, vol. 46, no. 1-2, pp. 1–184, 2001.

[67] O. D. Neikov, "Chapter 3—mechanical alloying," in *Handbook of Non-Ferrous Metal Powders*, O. D. Neikov, S. S. Naboychenko, and N. A. Yefimov, Eds., pp. 91–124, Elsevier, Oxford, UK, 2nd edition, 2019.

[68] J. B. Al-Dabbagh, R. M. Tahar, and S. Harun, "Structural and phase formation of TiAl alloys synthesized by mechanical alloying and heat treatment," *International Journal of Nanoelectronics and Materials*, vol. 8, pp. 23–32, 2015.

[69] S. K. Vajpai and K. Ameyama, "A novel powder metallurgy processing approach to prepare fine-grained Ti-rich TiAl-based alloys from pre-alloyed powders," *Intermetallics*, vol. 42, pp. 146–155, 2013.

[70] T. Shanmugasundaram, J. Guyon, J. P. Monchoux, A. Hazotte, and E. Bouzy, "On grain refinement of a γ-TiAl alloy using cryo-milling followed by spark plasma sintering," *Intermetallics*, vol. 66, pp. 141–148, 2015.

[71] K. H. Sim, G. Wang, J. M. Ju, J. Yang, and X. Li, "Microstructure and mechanical properties of a Ti–22Al–25Nb alloy fabricated from elemental powders by mechanical alloying and spark plasma sintering," *Journal of Alloys and Compounds*, vol. 704, pp. 425–433, 2017.

[72] H. Deng, A. Chen, L. Chen, Y. Wei, Z. Xia, and J. Tang, "Bulk nanostructured Ti-45Al-8Nb alloy fabricated by cryomilling and spark plasma sintering," *Journal of Alloys and Compounds*, vol. 772, pp. 140–149, 2019.

[73] J. Guyon, A. Hazotte, J. P. Monchoux, and E. Bouzy, "Effect of powder state on spark plasma sintering of TiAl alloys," *Intermetallics*, vol. 34, pp. 94–100, 2013.

[74] Y. Wang, C. Zhang, Y. Liu, S. Zhao, and J. Li, "Microstructure characterization and mechanical properties of TiAl-based alloys prepared by mechanical milling and spark plasma sintering," *Materials Characterization*, vol. 128, pp. 75–84, 2017.

[75] Z. Sun and H. Hashimoto, "Fabrication of TiAl alloys by MA-PDS process and the mechanical properties," *Intermetallics*, vol. 11, no. 8, pp. 825–834, 2003.

[76] W. Guo, A. Iasonna, M. Magini, S. Martelli, and F. Padella, "Synthesis of amorphous and metastable Ti40Al60 alloys by mechanical alloying of elemental powders," *Journal of Materials Science*, vol. 29, no. 9, pp. 2436–2444, 1994.

[77] M. S. El-Eskandarany, *Mechanical Alloying: Nanotechnology, Materials Science and Powder Metallurgy*, Elsevier, Oxford, UK, 2nd edition, 2015.

[78] H. Ghayour, M. Abdellahi, and M. Bahmanpour, "Optimization of the high energy ball-milling: modeling and parametric study," *Powder Technology*, vol. 291, pp. 7–13, 2016.

[79] C. J. da Rocha, R. M. L. Neto, V. S. Gonçalves, L. L. Carvalho, and F. A. Filho, "An investigation of the use of stearic acid as a process control agent in high energy ball milling of Nb-Al and Ni-Al powder mixtures," *Materials Science Forum*, vol. 416–418, pp. 144–149, 2003.

[80] A. Nouri and C. Wen, "Surfactants in mechanical alloying/milling: a catch-22 situation," *Critical Reviews in Solid State and Materials Sciences*, vol. 39, no. 2, pp. 81–108, 2014.

[81] W. Guo, S. Martelli, F. Padella et al., "F.C.C metastable phase induced in the Ti-Al system by mechanical alloying of pure elemental powders," *Materials Science Forum*, vol. 88–90, pp. 139–146, 1992.

[82] J. H. Ahn, H. Chung, R. Watanabe, and Y. H. Park, "Microstructural refinement & amorphisation in Ti-Al, Ti-Si and Si-W system by mechanical alloying," *Materials Science Forum*, vol. 88–90, pp. 347–354, 1992.

[83] W. Guo, S. Martelli, N. Burgio et al., "Mechanical alloying of the Ti-Al system," *Journal of Materials Science*, vol. 26, no. 22, pp. 6190–6196, 1991.

[84] Y. H. Park, H. Hashimoto, and R. Watanabe, "Morphological evolution and amorphization of Ti/Cu and Ti/Al powder mixtures during vibratory ball milling," *Materials Science Forum*, vol. 88–90, pp. 59–66, 1992.

[85] C. Suryanarayana, G.-H. Chen, A. Frefer, and F. H. Froes, "Structural evolution of mechanically alloyed Ti-Al alloys," *Materials Science and Engineering: A*, vol. 158, no. 1, pp. 93–101, 1992.

[86] Z. A. Munir, U. Anselmi-Tamburini, and M. Ohyanagi, "The effect of electric field and pressure on the synthesis and consolidation of materials: a review of the spark plasma sintering method," *Journal of Materials Science*, vol. 41, no. 3, pp. 763–777, 2006.

[87] M. Suárez, A. Fernández, J. Menéndez et al., "Challenges and opportunities for spark plasma sintering: a key technology for a new generation of materials," in *Sintering Applications*, pp. 319–342, IntechOpen, London, UK, 2013.

[88] R. Orru, R. Licheri, A. M. Locci, A. Cincotti, and G. Cao, "Consolidation/synthesis of materials by electric current activated/assisted sintering," *Materials Science and Engineering: R: Reports*, vol. 63, no. 4–6, pp. 127–287, 2009.

[89] W. Matizamhuka, "Spark plasma sintering (SPS)-an advanced sintering technique for structural nanocomposite materials," *Journal of the Southern African Institute of Mining and Metallurgy*, vol. 116, no. 7, pp. 1171–1180, 2016.

[90] M. A. Lagos and I. Agote, "SPS synthesis and consolidation of TiAl alloys from elemental powders: microstructure evolution," *Intermetallics*, vol. 36, pp. 51–56, 2013.

[91] D. Wang, H. Yuan, and J. Qiang, "The microstructure evolution, mechanical properties and densification mechanism of TiAl-based alloys prepared by spark plasma sintering," *Metals*, vol. 7, no. 6, p. 201, 2017.

[92] D. Wang, H. Zhao, and W. Zheng, "Effect of temperature-related factors on densification, microstructure and mechanical properties of powder metallurgy TiAl-based alloys," *Advanced Powder Technology*, 2019, in press.

[93] C. Zhang, K. Zhang, and G. Wang, "Dependence of heating rate in PCAS on microstructures and high temperature deformation properties of γ-TiAl intermetallic alloys," *Intermetallics*, vol. 18, no. 5, pp. 834–840, 2010.

[94] S. Diouf and A. Molinari, "Densification mechanisms in spark plasma sintering: effect of particle size and pressure," *Powder Technology*, vol. 221, pp. 220–227, 2012.

[95] J. E. Garay, "Current-activated, pressure-assisted densification of materials," *Annual Review of Materials Research*, vol. 40, no. 1, pp. 445–468, 2010.

[96] Z. Trzaska, A. Couret, and J.-P. Monchoux, "Spark plasma sintering mechanisms at the necks between TiAl powder particles," *Acta Materialia*, vol. 118, pp. 100–108, 2016.

[97] Y. Chen, H. Yu, D. Zhang, and L. Chai, "Effect of spark plasma sintering temperature on microstructure and mechanical properties of an ultrafine grained TiAl intermetallic alloy," *Materials Science and Engineering: A*, vol. 525, no. 1-2, pp. 166–173, 2009.

[98] Y. H. Wang, J. P. Lin, Y. H. He, Y. L. Wang, and G. L. Chen, "Microstructures and mechanical properties of Ti–45Al–8.5Nb–(W, B, Y) alloy by SPS–HIP route," *Materials Science and Engineering: A*, vol. 489, no. 1-2, pp. 55–61, 2008.

[99] Y. H. Wang, J. P. Lin, Y. H. He, Y. L. Wang, and G. L. Chen, "Fabrication and SPS microstructures of Ti–45Al–8.5Nb–(W, B, Y) alloying powders," *Intermetallics*, vol. 16, no. 2, pp. 215–224, 2008.

[100] H. Jabbar, A. Couret, L. Durand, and J.-P. Monchoux, "Identification of microstructural mechanisms during densification of a TiAl alloy by spark plasma sintering," *Journal of Alloys and Compounds*, vol. 509, no. 41, pp. 9826–9835, 2011.

[101] H. T. Wu, Y. L. Yue, W. B. Wu, and H. Y. Yin, "Fabrication of TiAl intermetallic by spark plasma sintering," in *Key Engineering Materials*, pp. 1050–1052, Trans Tech Publications Inc, Zürich, Switzerland, 2007.

[102] T. Rudolf, B. Skrotzki, and G. Eggeler, "Microstructural evolution during creep of a duplex near-γ TiAl-Alloy," *Materials Science and Engineering: A*, vol. 319–321, pp. 815–819, 2001.

[103] P. Dumitraschkewitz, H. Clemens, S. Mayer, and D. Holec, "Impact of alloying on stacking fault energies in γ-TiAl," *Applied Sciences*, vol. 7, no. 11, p. 1193, 2017.

[104] A. Couret, "Glide mechanism of ordinary dislocations in the γ phase of TiAl," *Intermetallics*, vol. 9, no. 10-11, pp. 899–906, 2001.

[105] J.-P. Monchoux, J. Luo, T. Voisin, and A. Couret, "Deformation modes and size effect in near-γ TiAl alloys," *Materials Science and Engineering: A*, vol. 679, pp. 123–132, 2017.

[106] I. H. Katzarov and A. T. Paxton, "Is the pinning of ordinary dislocations in γ-TiAl intrinsic or extrinsic in nature? A combined atomistic and kinetic Monte Carlo approach," *Acta Materialia*, vol. 59, no. 3, pp. 1281–1290, 2011.

[107] E. Tadmor and N. Bernstein, "A first-principles measure for the twinnability of FCC metals," *Journal of the Mechanics and Physics of Solids*, vol. 52, no. 11, pp. 2507–2519, 2004.

[108] B. Liu, Y. Liu, Y. P. Li, W. Zhang, and A. Chiba, "Thermomechanical characterization of β-stabilized Ti–45Al–7Nb–0.4W–0.15B alloy," *Intermetallics*, vol. 19, no. 8, pp. 1184–1190, 2011.

[109] I. H. Katzarov and A. T. Paxton, "Atomistic studies of interactions between the dominant lattice dislocations and γ/γ-lamellar boundaries in lamellar γ-TiAl," *Acta Materialia*, vol. 57, no. 11, pp. 3349–3366, 2009.

[110] V. Vitek, "Atomic level computer modelling of crystal defects with emphasis on dislocations: past, present and future," *Progress in Materials Science*, vol. 56, no. 6, pp. 577–585, 2011.

[111] M. Kanani, A. Hartmaier, and R. Janisch, "Stacking fault based analysis of shear mechanisms at interfaces in lamellar TiAl alloys," *Acta Materialia*, vol. 106, pp. 208–218, 2016.

[112] T. E. J. Edwards, F. Di Gioacchino, A. J. Goodfellow, and W. J. Clegg, "Slip bands in lamellar TiAl during high cycle fatigue microcompression by correlative total strain mapping, diffraction orientation mapping and transmission electron imaging," *International Journal of Fatigue*, vol. 124, pp. 520–527, 2019.

[113] T. E. J. Edwards, F. Di Gioacchino, A. J. Goodfellow et al., "Transverse deformation of a lamellar TiAl alloy at high temperature by in situ microcompression," *Acta Materialia*, vol. 166, pp. 85–99, 2019.

[114] T. E. J. Edwards, F. Di Gioacchino, G. Mohanty, J. Wehrs, J. Michler, and W. J. Clegg, "Longitudinal twinning in a TiAl alloy at high temperature by in situ microcompression," *Acta Materialia*, vol. 148, pp. 202–215, 2018.

[115] T. E. J. Edwards, F. Di Gioacchino, R. Muñoz-Moreno, and W. J. Clegg, "Deformation of lamellar TiAl alloys by longitudinal twinning," *Scripta Materialia*, vol. 118, pp. 46–50, 2016.

[116] S. Naanani, J.-P. Monchoux, C. Mabru, and A. Couret, "Pure climb of [001] dislocations in TiAl at 850°C," *Scripta Materialia*, vol. 149, pp. 53–57, 2018.

[117] B. Skrotzki, T. Rudolf, A. Dlouhy, and G. Eggeler, "Microstructural evidence for dynamic recrystallization during creep of a duplex near-γ TiAl-alloy," *Scripta Materialia*, vol. 39, no. 11, pp. 1545–1551, 1998.

[118] F. J. Humphreys and M. Hatherly, *Recrystallization and Related Annealing Phenomena*, Elsevier, Amsterdam, Netherlands, 2012.

[119] G. Wang, L. Xu, Y. Tian, Z. Zheng, Y. Cui, and R. Yang, "Flow behavior and microstructure evolution of a P/M TiAl alloy during high temperature deformation," *Materials Science and Engineering: A*, vol. 528, no. 22-23, pp. 6754–6763, 2011.

[120] T. Schmoelzer, K.-D. Liss, P. Staron, S. Mayer, and H. Clemens, "The contribution of high-energy X-rays and neutrons to characterization and development of intermetallic titanium aluminides," *Advanced Engineering Materials*, vol. 13, no. 8, pp. 685–699, 2011.

[121] F. Godor, R. Werner, J. Lindemann, H. Clemens, and S. Mayer, "Characterization of the high temperature deformation behavior of two intermetallic TiAl–Mo alloys," *Materials Science and Engineering: A*, vol. 648, pp. 208–216, 2015.

[122] R. M. Imayev, V. M. Imayev, M. Oehring, and F. Appel, "Microstructural evolution during hot working of Ti aluminide alloys: influence of phase constitution and initial casting texture," *Metallurgical and Materials Transactions A*, vol. 36, no. 13, pp. 859–867, 2005.

[123] L. Cheng, H. Chang, B. Tang, H. Kou, and J. Li, "Deformation and dynamic recrystallization behavior of a high Nb containing TiAl alloy," *Journal of Alloys and Compounds*, vol. 552, pp. 363–369, 2013.

[124] L. Xiang, B. Tang, X. Xue, H. Kou, and J. Li, "Microstructural characteristics and dynamic recrystallization behavior of β-γ TiAl based alloy during high temperature deformation," *Intermetallics*, vol. 97, pp. 52–57, 2018.

[125] Y. Y. Luo, Z. P. Xi, W. D. Zeng, X. N. Mao, Y. L. Yang, and H. Z. Niu, "Characteristics of high-temperature deformation behavior of Ti–45Al–2Cr–3Ta–0.5W alloy," *Journal of Materials Engineering and Performance*, vol. 23, no. 10, pp. 3577–3585, 2014.

[126] H. Li, Z. Li, W. Zhang, Y. Wang, Y. Liu, and H. Wang, "High temperature deformability and microstructural evolution of Ti–47Al–2Cr–0.2Mo alloy," *Journal of Alloys and Compounds*, vol. 508, no. 2, pp. 359–363, 2010.

[127] N. Cui, F. Kong, X. Wang, Y. Chen, and H. Zhou, "Hot deformation behavior and dynamic recrystallization of a β-solidifying TiAl alloy," *Materials Science and Engineering: A*, vol. 652, pp. 231–238, 2016.

[128] Y. Hao, J. Liu, S. Li, J. Li, X. Liu, and X. Feng, "Effects of nano-twinning on the deformation and mechanical behaviours of TiAl alloys with distinct microstructure at elevated loading temperatures," *Materials Science and Engineering: A*, vol. 705, pp. 210–218, 2017.

[129] Y. V. R. K. Prasad, H. L. Gegel, S. M. Doraivelu et al., "Modeling of dynamic material behavior in hot deformation: forging of Ti-6_{242}," *Metallurgical Transactions A*, vol. 15, no. 10, pp. 1883–1892, 1984.

[130] Y. Sun, Z. Wan, L. Hu, and J. Ren, "Characterization of hot processing parameters of powder metallurgy TiAl-based alloy based on the activation energy map and processing map," *Materials & Design*, vol. 86, pp. 922–932, 2015.

[131] X. Ma, W. Zeng, F. Tian, Y. Zhou, and Y. Sun, "Optimization of hot process parameters of Ti–6.7Al–2Sn–2.2Zr–2.1Mo–1W–0.2Si alloy with lamellar starting microstructure based on the processing map," *Materials Science and Engineering: A*, vol. 545, pp. 132–138, 2012.

[132] H. Zhou, Q. D. Wang, B. Ye, and W. Guo, "Hot deformation and processing maps of as-extruded Mg–9.8Gd–2.7Y–0.4Zr Mg alloy," *Materials Science and Engineering: A*, vol. 576, pp. 101–107, 2013.

[133] M. Karami and R. Mahmudi, "Hot shear deformation constitutive analysis and processing map of extruded Mg–12Li–1Zn bcc alloy," *Materials & Design*, vol. 53, pp. 534–539, 2014.

[134] H. Sun, Y. Sun, R. Zhang, M. Wang, R. Tang, and Z. Zhou, "Study on hot workability and optimization of process parameters of a modified 310 austenitic stainless steel using processing maps," *Materials & Design*, vol. 67, pp. 165–172, 2015.

[135] G. Liu, Y. Han, Z. Shi, J. Sun, D. Zou, and G. Qiao, "Hot deformation and optimization of process parameters of an as-cast 6Mo superaustenitic stainless steel: a study with processing map," *Materials & Design*, vol. 53, pp. 662–672, 2014.

[136] W. Peng, W. Zeng, Q. Wang, and H. Yu, "Characterization of high-temperature deformation behavior of as-cast Ti60 titanium alloy using processing map," *Materials Science and Engineering: A*, vol. 571, pp. 116–122, 2013.

[137] Y. Prasad, K. Rao, and S. Sasidhar, *Hot Working Guide: A Compendium of Processing Maps*, ASM international, Cleveland, OH, USA, 2015.

[138] Y. Prasad and T. Seshacharyulu, "Processing maps for hot working of titanium alloys," *Materials Science and Engineering A*, vol. 243, no. 1-2, pp. 82–88, 1998.

[139] G. E. Dieter, H. A. Kuhn, and S. L. Semiatin, *Handbook of Workability and Process Design*, ASM international, Cleveland, OH, USA, 2003.

[140] Y. V. R. K. Prasad, "Processing maps: a status report," *Journal of Materials Engineering and Performance*, vol. 12, no. 6, pp. 638–645, 2003.

[141] K. P. Rao, Y. V. R. K. Prasad, and K. Suresh, "Hot working behavior and processing map of a γ-TiAl alloy synthesized by powder metallurgy," *Materials & Design*, vol. 32, no. 10, pp. 4874–4881, 2011.

[142] Y. Chu, J. Li, F. Zhao, B. Tang, and H. Kou, "Characterization of the elevated temperature compressive deformation behavior of high Nb containing TiAl alloys with two microstructures," *Materials Science and Engineering: A*, vol. 725, pp. 466–478, 2018.

[143] Z. Wan, Y. Sun, L. Hu, and H. Yu, "Experimental study and numerical simulation of dynamic recrystallization behavior of TiAl-based alloy," *Materials & Design*, vol. 122, pp. 11–20, 2017.

[144] Z. Wan, Y. Sun, L. Hu, and H. Yu, "Dynamic softening behavior and microstructural characterization of TiAl-based alloy during hot deformation," *Materials Characterization*, vol. 130, pp. 25–32, 2017.

[145] Y. Xu, L. Hu, and Y. Sun, "Deformation behaviour and dynamic recrystallization of AZ61 magnesium alloy," *Journal of Alloys and Compounds*, vol. 580, pp. 262–269, 2013.

[146] X.-P. Liang, Y. Liu, H.-Z. Li, C.-X. Zhou, and G.-F. Xu, "Constitutive relationship for high temperature deformation of powder metallurgy Ti–47Al–2Cr–2Nb–0.2W alloy," *Materials & Design*, vol. 37, pp. 40–47, 2012.

[147] X. He, Z. Yu, and X. Lai, "Analysis of high temperature deformation behavior of a high Nb containing TiAl based alloy," *Materials Letters*, vol. 62, no. 26, pp. 4181–4183, 2008.

[148] D.-Y. Zhang, H.-Z. Li, X.-P. Liang, Z.-W. Wei, and Y. Liu, "Microstructure characteristic for high temperature deformation of powder metallurgy Ti–47Al–2Cr–0.2Mo alloy," *Materials & Design*, vol. 59, pp. 415–420, 2014.

[149] J. Xin, L. Zhang, G. Ge, and J. Lin, "Characterization of microstructure evolution in β-γ TiAl alloy containing high content of Niobium using constitutive equation and power dissipation map," *Materials & Design*, vol. 107, pp. 406–415, 2016.

[150] M. Thomas and M.-P. Bacos, "Processing and characterization of TiAl-based alloys: towards an industrial scale," *AerospaceLab*, vol. 3, pp. 1–11, 2011.

[151] J. Dai, J. Zhu, C. Chen, and F. Weng, "High temperature oxidation behavior and research status of modifications on improving high temperature oxidation resistance of titanium alloys and titanium aluminides: a review," *Journal of Alloys and Compounds*, vol. 685, pp. 784–798, 2016.

[152] C. Leyens, "Oxidation and protection of titanium alloys and titanium aluminides," in *Titanium and Titanium Alloys. Fundamentals and Applications*, C. Leyens and M. Peters, Eds., pp. 187–223, Wiley-VCH Verlag GmbH & Co. KGaA, Weinheim, Germany, 2003.

[153] Y. Song, J. Dai, and R. Yang, "Mechanism of oxygen adsorption on surfaces of γ-TiAl," *Surface Science*, vol. 606, no. 9-10, pp. 852–857, 2012.

[154] Y. Song, F. J. Xing, J. H. Dai, and R. Yang, "First-principles study of influence of Ti vacancy and Nb dopant on the bonding of TiAl/TiO_2 interface," *Intermetallics*, vol. 49, pp. 1–6, 2014.

[155] D. Pilone and F. Felli, "Isothermal oxidation behaviour of TiAl–Cr–Nb–B alloys produced by induction melting," *Intermetallics*, vol. 26, pp. 36–39, 2012.

[156] F.-P. Ping, Q.-M. Hu, A. V. Bakulin, S. E. Kulkova, and R. Yang, "Alloying effects on properties of Al_2O_3 and TiO_2 in connection with oxidation resistance of TiAl," *Intermetallics*, vol. 68, pp. 57–62, 2016.

[157] J. Dai, J. Zhu, L. Zhuang, and S. Li, "Effect of surface aluminizing on long-term high-temperature thermal stability of TC4 titanium alloy," *Surface Review and Letters*, vol. 23, no. 2, Article ID 1550102, 2016.

[158] Y. Shida and H. Anada, "Oxidation behavior of binary Ti–Al alloys in high temperature air environment," *Materials Transactions, JIM*, vol. 34, no. 3, pp. 236–242, 1993.

[159] W. Lu, C. Chen, Y. Xi, C. Guo, F. Wang, and L. He, "TEM investigation of the oxide scale of Ti–46.5Al–5Nb at 900°C for 50 h," *Intermetallics*, vol. 15, no. 5-6, pp. 824–831, 2007.

[160] M. Yoshihara and Y.-W. Kim, "Oxidation behavior of gamma alloys designed for high temperature applications," *Intermetallics*, vol. 13, no. 9, pp. 952–958, 2005.

[161] V. A. C. Haanappel, H. Clemens, and M. F. Stroosnijder, "The high temperature oxidation behaviour of high and low alloyed TiAl-based intermetallics," *Intermetallics*, vol. 10, no. 3, pp. 293–305, 2002.

[162] S. Taniguchi and T. Shibata, "Influence of additional elements on the oxidation behaviour of TiAl," *Intermetallics*, vol. 4, pp. S85–S93, 1996.

[163] R. Braun, M. Fröhlich, C. Leyens, and D. Renusch, "Oxidation behaviour of TBC systems on γ-TiAl based alloy Ti–45Al–8Nb," *Oxidation of Metals*, vol. 71, no. 5-6, p. 295, 2009.

[164] Z. W. Huang and T. Cong, "Microstructural instability and embrittlement behaviour of an Al-lean, high-Nb γ-TiAl-based alloy subjected to a long-term thermal exposure in air," *Intermetallics*, vol. 18, no. 1, pp. 161–172, 2010.

[165] J. P. Lin, L. L. Zhao, G. Y. Li et al., "Effect of Nb on oxidation behavior of high Nb containing TiAl alloys," *Intermetallics*, vol. 19, no. 2, pp. 131–136, 2011.

[166] X. Cheng, X. Wan, and J. Shen, "The effect of Nb on the oxidation behaviour of TiAl alloy at high temperature," *Journal of Chinese Society for Corrosion and Protection*, vol. 22, no. 2, pp. 69–71, 2009.

[167] Y. Shida and H. Anada, "The influence of ternary element addition on the oxidation behaviour of TiAl intermetallic compound in high temperature air," *Corrosion Science*, vol. 35, no. 5–8, pp. 945–953, 1993.

[168] D. W. McKee and S. C. Huang, "The oxidation behavior of gamma-titanium aluminide alloys under thermal cycling conditions," *Corrosion Science*, vol. 33, no. 12, pp. 1899–1914, 1992.

[169] I. C. I. Okafor and R. G. Reddy, "The oxidation behavior of high-temperature aluminides," *JOM*, vol. 51, no. 6, pp. 35–40, 1999.

[170] R. G. Reddy, Y. Li, and M. F. Arenas, "Oxidation of a ternary Ti_3Al-Ta alloy," *High Temperature Materials and Processes*, vol. 21, no. 4, pp. 195–206, 2002.

[171] T. Popela, D. Vojtěch, P. Novák et al., "High-temperature oxidation of Ti-Al-Ta and Ti-Al-Nb alloys," *Metal*, vol. 18, pp. 1–4, 2010.

[172] D. Vojtěch, T. Popela, J. Kubásek, J. Maixner, and P. Novák, "Comparison of Nb-and Ta-effectiveness for improvement of the cyclic oxidation resistance of TiAl-based intermetallics," *Intermetallics*, vol. 19, no. 4, pp. 493–501, 2011.

[173] L. Yuanyuan, Z. Weidong, X. Zhengping et al., "Microstructure, mechanical properties and oxidation behavior of a

hot-extruded TiAl containing Ta," *Rare Metal Materials and Engineering*, vol. 44, no. 2, pp. 282–287, 2015.

[174] M. Mitoraj and E. M. Godlewska, "Oxidation of Ti-46Al-8Ta in air at 700°C and 800°C under thermal cycling conditions," *Intermetallics*, vol. 34, pp. 112–121, 2013.

[175] Z. Y. He, Z. X. Wang, F. Zhang, Z. Y. Wang, and X. P. Liu, "Oxidation behavior of TiAl alloy treated by plasma surface chromizing process," *Surface and Coatings Technology*, vol. 228, no. S1, pp. S287–S291, 2013.

[176] R. Peter, I. Saric, I. K. Piltaver, I. J. Badovinac, and M. Petravic, "Oxide formation on chromium metal surfaces by low-energy oxygen implantation at room temperature," *Thin Solid Films*, vol. 636, pp. 225–231, 2017.

[177] D. Kim, D. Seo, X. Huang et al., "Oxidation behaviour of gamma titanium aluminides with or without protective coatings," *International Materials Reviews*, vol. 59, no. 6, pp. 297–325, 2014.

[178] N. Sruthi Neelam, S. Banumathy, A. Bhattacharjee, and G. V. S. NageswaraRao, "The effect of Cr and Mo addition on the oxidation behaviour of Ti-46.5Al-3.5Nb-2Cr-0.3B," *Materials Today: Proceedings*, vol. 15, pp. 30–35, 2019.

[179] L. L. Zhao, G. Y. Li, L. Q. Zhang et al., "Influence of Y addition on the long time oxidation behaviors of high Nb containing TiAl alloys at 900°C," *Intermetallics*, vol. 18, no. 8, pp. 1586–1596, 2010.

[180] Y. Wu, S. K. Hwang, S. W. Nam, and N. J. Kim, "The effect of yttrium addition on the oxidation resistance of EPM TiAl-based intermetallics," *Scripta Materialia*, vol. 48, no. 12, pp. 1655–1660, 2003.

[181] Y. Wu, K. Hagihara, and Y. Umakoshi, "Influence of Y-addition on the oxidation behavior of Al-rich γ-TiAl alloys," *Intermetallics*, vol. 12, no. 5, pp. 519–532, 2004.

[182] L. L. Xiang, L. L. Zhao, Y. L. Wang, L. Q. Zhang, and J. P. Lin, "Synergistic effect of Y and Nb on the high temperature oxidation resistance of high Nb containing TiAl alloys," *Intermetallics*, vol. 27, pp. 6–13, 2012.

[183] X. Gong, R. R. Chen, H. Z. Fang et al., "Synergistic effect of B and Y on the isothermal oxidation behavior of TiAl-Nb-Cr-V alloy," *Corrosion Science*, vol. 131, pp. 376–385, 2018.

[184] A. Donchev, E. Richter, M. Schütze, and R. Yankov, "Improvement of the oxidation behaviour of TiAl-alloys by treatment with halogens," *Intermetallics*, vol. 14, no. 10-11, pp. 1168–1174, 2006.

[185] A. Donchev and M. Schütze, "Improving the oxidation resistance of γ-titanium aluminides by halogen treatment," *Materials and Corrosion*, vol. 59, no. 6, pp. 489–493, 2008.

[186] P. J. Masset, S. Neve, H.-E. Zschau, and M. Schütze, "Influence of alloy compositions on the halogen effect in TiAl alloys," *Materials and Corrosion*, vol. 59, no. 7, pp. 609–618, 2008.

[187] P. J. Masset and M. Schütze, "Thermodynamic assessment of the alloy concentration limits for the halogen effect of TiAl alloys," *Advanced Engineering Materials*, vol. 10, no. 7, pp. 666–674, 2008.

[188] M.-H. Mo, L.-K. Wu, H.-Z. Cao, J.-P. Lin, and G.-Q. Zheng, "Halogen effect for improving high temperature oxidation resistance of Ti-50Al by anodization," *Applied Surface Science*, vol. 407, pp. 246–254, 2017.

[189] G. Schumacher, F. Dettenwanger, M. Schütze et al., "Microalloying effects in the oxidation of TiAl materials," *Intermetallics*, vol. 7, no. 10, pp. 1113–1120, 1999.